



Title	Freezing, Melting, and Light Stress on the Photophysiology of Ice Algae: Ex Situ Incubation of the Ice Algal diatom <i>Fragilariopsis cylindrus</i> (Bacillariophyceae) Using an Ice Tank
Author(s)	Yoshida, Kazuhiro; Seger, Andreas; Kennedy, Fraser; McMinn, Andrew; Suzuki, Koji
Citation	Journal of Phycology, 56(5), 1323-1338 https://doi.org/10.1111/jpy.13036
Issue Date	2020-10
Doc URL	http://hdl.handle.net/2115/82871
Rights	This is the peer reviewed version of the following article: Yoshida, K. Seger, A. Kennedy, F. McMinn, A. Suzuki, K. Freezing, Melting, and Light Stress on the Photophysiology of Ice Algae: Ex Situ Incubation of the Ice Algal diatom <i>Fragilariopsis cylindrus</i> (Bacillariophyceae) Using an Ice Tank. Journal of Phycology. 2020; 56(5): 1323-1338, which has been published in final form at https://doi.org/10.1111/jpy.13036 . This article may be used for non-commercial purposes in accordance with Wiley Terms and Conditions for Use of Self-Archived Versions.
Type	article (author version)
Additional Information	There are other files related to this item in HUSCAP. Check the above URL.
File Information	Yoshida et al. Accepted_JPhycol.pdf



[Instructions for use](#)

1 FREEZING, MELTING AND LIGHT STRESS ON THE PHOTOPHYSIOLOGY OF
2 ICE ALGAE: *EX SITU* INCUBATION OF THE ICE ALGAL DIATOM
3 *FRAGILARIOPSIS CYLINDRUS* (BACILLARIOPHYCEAE) USING AN ICE TANK¹

4

5 Kazuhiro Yoshida

6 Graduate School of Environmental Science, Hokkaido University, North 10 West 5,

7 Kita-Ku, Sapporo, Hokkaido 060-0810 Japan

8 Institute for Marine and Antarctic Studies, University of Tasmania, 20 Castray

9 Esplanade, Battery Point TAS 7004 Australia

10

11 Andreas Seger

12 Institute for Marine and Antarctic Studies, University of Tasmania, 20 Castray

13 Esplanade, Battery Point TAS 7004 Australia

14 South Australian Research and Development Institute, 2b Hartley Grove, Urrbrae, SA,

15 5064 Australia

16

17

Fraser Kennedy, Andrew McMinn²

18

Institute for Marine and Antarctic Studies, University of Tasmania, 20 Castray

19

Esplanade, Battery Point TAS 7004 Australia

20

21

and Koji Suzuki

22

Faculty of Environmental Earth Science, Hokkaido University, North 10 West 5, Kita-

23

Ku, Sapporo, Hokkaido 060-0810 Japan

24

25 ¹ Submitted 24/06/2019

26 ² Author for correspondence:

27 Andrew McMinn

28 Tel: +61- 3 6226 6379

29 E-mail: Andrew McMinn@utas.edu.au

30

31 RUNNING HEAD: Ice algal physiology in an ice tank

32

33 KEYWORDS: active chl *a* fluorescence; algal pigments; ice tank incubation;

34 photoprotection; *psbA*; *rbcL*; sea ice

35

36 ABBREVIATIONS:

37 cDNA, complementary DNA; Chl *a*, chlorophyll *a*; ChlF, active chlorophyll *a*

38 fluorescence; DD, diadinoxanthin; DT, diatoxanthin; DES, de-epoxidation state index

39 of DD-DD xanthophyll cycle; ETR, electron transport rate; Fe⁰, inorganic Fe species;

40 FRRf, fast repetition rate fluorometry; HL, high light; LL, low light; NPQ, non-

41 photochemical quenching; PQ, plastoquinone; *PP*, primary productivity; PPC,

42 photoprotective carotenoid; PSC, photosynthetic carotenoid; Q_A, the first quinone

43 electron acceptor; Q_B, secondary quinone electron acceptor; Tchl *a*, total chl *a*;

44 UHPLC, ultra-high performance liquid chromatography

45

46 ABSTRACT

47 Sea-ice algae contribute up to 25% of the primary productivity of polar seas and seed
48 large-scale ice-edge blooms. Fluctuations in temperature, salinity, and light associated
49 with the freeze/thaw cycle can significantly impact the photophysiology of ice-
50 associated taxa. The effects of multiple co-stressors (i.e., freezing temperature and high
51 brine salinity or sudden high light exposure) on the photophysiology of ice algae were
52 investigated in a series of ice tank experiments with the polar diatom *Fragilariopsis*
53 *cylindrus* under different light intensities. When algal cells were frozen into the ice, the
54 maximum quantum yield of photosystem II photochemistry (PSII) (F_v/F_m) decreased
55 possibly due to the damage of PSII reaction centres and/or high brine salinity stress
56 suppressing the reduction capacity downstream of PSII. Expression of the *rbcL* gene
57 was highly upregulated, suggesting that cells initiated strategies to enhance survival
58 upon freezing in. Algae contained within the ice-matrix displayed similar levels of
59 F_v/F_m regardless of the light treatments. Upon melting out, cells were exposed to high
60 light ($800 \mu\text{mol photons m}^{-2} \text{s}^{-1}$), resulting in a rapid decline in F_v/F_m and significant
61 upregulation of non-photochemical quenching (NPQ). These results suggest that ice
62 algae employed safety valves (i.e., NPQ) to maintain their photosynthetic capability
63 during the sudden environmental changes. Our results infer that sea ice algae are highly
64 adaptable when exposed to multiple co-stressors and that their success can, in part, be

- 65 explained by the ability to rapidly modify their photosynthetic competence; a key factor
- 66 contributing to algal bloom formation in the polar seas.

67 INTRODUCTION

68 Sea ice algae are significant primary producers in sea ice zones. They contribute
69 5–25% of the total primary production (*PP*) in seasonally ice-covered regions
70 (Legendre et al. 1992, Lizotte 2001, Michel et al. 2006, Loose et al. 2011, Arrigo 2017)
71 and ~50% of the annual *PP* in perennially ice-covered regions (Satoh et al. 1989,
72 McMinn et al. 2010, Fernandez-Mendez et al. 2015). Ice-associated algae are of high
73 ecological importance as not only the primary energy source for sea ice biota such as
74 zooplankton, krill, larval fish and benthos (Lizotte 2001, Boetius et al. 2013, 2015,
75 Kohlbach et al. 2017, Moteki et al. 2017, Bernard et al. 2018) but also as seed biomass
76 for ice-edge blooms in marginal sea ice zones (e.g., Smith and Nelson 1986, Syvertsen
77 1991, Arrigo and van Dijken 2003, Arrigo 2014). Ice-edge blooms, which ice algae may
78 seed, contribute ~50% of the total *PP* in marginal sea ice zone of the Southern Ocean
79 (Smith and Nelson 1986, Sakshaug and Slagstad 1991, Deppeler and Davidson 2017),
80 although it is still controversial which ice algae or phytoplankton actually contribute to
81 the blooms (see review of van Leeuwe et al. 2018). Upon freezing in, algae can form
82 aggregates within microstructures of the ice, which channel excluded liquid brine from
83 sea ice to under-ice seawater when ice grows (i.e., brine channels) (Melnikov and
84 Bondarchuk 1987, Assmy et al. 2013, Boetius et al. 2013, Katlein et al. 2015,

85 Fernandez-Mendez et al. 2014, Boetius et al. 2015). During the sea ice melt, these algal
86 aggregates can rapidly sink and transport carbon down to the sea floor. This process
87 contributes to the biological carbon pump (Riebesell et al. 1991, Taguchi et al. 1997,
88 Boetius et al. 2013, Katlein et al. 2015) and underlines the important contribution of ice
89 algae to both the ecology and biogeochemistry of sea ice zones. It is thus important to
90 understand how ice algae survive in the dynamic and heterogeneous sea ice
91 environment. Sea ice environments are subject to large fluctuations in temperature
92 (~ -20 °C to -1.8 °C; Petrich and Eicken 2017), salinity (~ 25 to 170; Arrigo et al. 2010)
93 and light availability (~ 0 to $1000 \mu\text{mol photons m}^{-2} \text{ s}^{-1}$; Galindo et al. 2017). Variation
94 in these abiotic parameters can influence the photosynthetic efficiency of ice algae,
95 however, they are not independent (i.e. multiple co-stressors; McMinn et al. 2017). Few
96 studies have addressed the influence of multiple co-stressors on the photophysiology of
97 sea ice algae (Ralph et al. 2005, 2007, Ryan et al. 2011, Martin et al. 2011, McMinn et
98 al. 2014; see review of McMinn 2017), and little is known about how co-stressors
99 influence ice algal photosynthesis and production during freeze/thaw cycles (McMinn
100 2017). Despite their significant ecological and biogeochemical importance, it remains
101 difficult to directly obtain the photophysiological properties of sea ice taxa *in situ*.
102 Kennedy et al. (2012) were the first to use sea ice tanks to undertake short-term

103 incubation of the haptophyte *Phaeocystis antarctica* within the laboratory. This method
104 has the advantage that ice algae can be incubated in an environment mimicking pack ice
105 conditions. Although many studies have addressed ice algal photosynthesis and
106 production using isolates resuspended in water (e.g., Yan et al. 2019), it remains
107 difficult to incubate them in the laboratory (e.g. in a culturing flask), while simulating
108 realistic environmental conditions. Using a previous ice tank model, Kennedy et al.
109 (2012) found that a freezing event suppressed the photochemical efficiency of PSII.
110 Although these experiments were able to reveal the effects of freezing on the
111 photophysiology of ice algae, their short-term nature did not address the longer-term
112 mechanism of freezing stress. Understanding how ice algae maintain photosynthetic
113 capacity and survive during freeze/thaw cycles is of considerable importance to better
114 assess primary productivity in sea ice environments. In this study, a novel 70 L ice tank
115 was constructed for the long-term incubation of ice algae under ecologically realistic
116 conditions. It was used to investigate the effects of multiple co-stressors on ice algal
117 photophysiology:

- 118 (1) freezing stress with low temperature and high brine salinity;
- 119 (2) chronic low light availability under low temperature and high salinity;

120 (3) melting stress with exposure to less saline meltwaters and sudden increase in light.

121 The sea ice diatom *Fragilariopsis cylindrus* was maintained in the ice tank for 20 days
122 followed by ice melt and light exposure experiments to reproduce the environment that
123 released ice algae experience. This study aims to investigate the effects of multiple co-
124 stressors on ice algal photophysiology in an artificial sea ice environment during a
125 freeze/thaw cycle. It provides new insights into how ice algae are able to tolerate
126 environmental fluctuations that contribute to their dominance of ice-edge blooms.

127

128 MATERIALS AND METHODS

129 *Ice tank incubation*

130 The polar pennate diatom *Fragilariopsis cylindrus* (isolated from Antarctic sea ice in
131 2015, Davis station, East Antarctica; Kennedy et al. 2019), was incubated in a purpose
132 designed ice tank (Island Research, Tasmania). The algal culture was less than two
133 years old at the start of the experiments. The ice tank was contained within a freezer (–
134 20 °C), and the ice thickness and temperature gradient of the ice were controlled by
135 interactions between a basal heater and the adjustable ambient freezer temperature (Fig.
136 1). This enabled an ice thickness of approximately 5.5 cm to be maintained during the
137 experiment. *F. cylindrus* was incubated in Aquil media (Price et al. 1989), buffered with

138 ethylenediaminetetraacetic acid (EDTA) (final concentration 5.00 μM) at a salinity of
139 35, and a Fe concentration of 400 nM. The concentration of total inorganic forms of Fe
140 ($\text{Fe}^{\text{'}}$) was 1.54 nM, this being continuously supplied from the Fe-EDTA complexes to
141 the medium calculated using the software Visual MINTEQ, ver. 3.1
142 (<https://vminteq.lwr.kth.se>). Light intensities beneath the ice, measured with a spherical
143 photosynthetically active radiation (PAR) sensor (QSL-100, Biospherical Instrument
144 Inc.), were set at 150 and 30 $\mu\text{mol photons m}^{-2} \text{s}^{-1}$ (White LED, PANEL-300-18W,
145 LED Lighting Products, Australia; Fig. S1) as high and low light (HL and LL)
146 treatments, respectively. Two discrete ice tank runs were conducted for each light
147 treatment. The diatom *F. cylindrus* was inoculated with low cell densities (HL: $4011 \pm$
148 $151 \text{ cells mL}^{-1}$; LL: $3933 \pm 132 \text{ cells mL}^{-1}$) to avoid the possibilities of self-shading
149 and nutrient starvation during the incubation experiments. They were maintained in the
150 ice tank for 3 days for acclimation where seawater temperature was maintained at 2.5
151 $^{\circ}\text{C}$. Prior to freezing in, a sample was taken to assess the original physiological state of
152 the algae (day -05, hereafter). The temperature lowered to $-1.8 \text{ }^{\circ}\text{C}$ to initiate ice
153 formation. Once ice had formed after 3 days, the under-ice water was partially replaced
154 with ultrapure water to reduce the salinity down to 35; as the salinity of the underlying
155 water had increased (to ~ 38) as a result of brine rejection. Two-day acclimation period

156 was used prior to sampling. Ice sampling was conducted every 5 days for 20 days (days
157 00, 05, 10, 15, and 20). Brine salinity and brine fraction were estimated following Cox
158 and Weeks (1983) and Eicken (2009). To minimize heterogeneity among ice cores, ice
159 samples were randomly collected from the tank chamber (pseudo-replicate) with a trace
160 metal-free hand drill (2 cm in diameter) from randomly annotated grids on the ice
161 surface, following normal random sampling numbers generated by the software R
162 (<https://www.r-project.org/>). To assess both the effects of melting and high light
163 exposure, ice samples were melted at 2.5 °C and salinity 25 for 2 days (melt samples,
164 hereafter). The melt samples were then exposed to intense light (light samples,
165 hereafter) ($800 \mu\text{mol photons m}^{-2} \text{s}^{-1}$) to mimick the typical summer surface
166 (MODIS/Aqua).

167

168 *Fast repetition rate (FRR) fluorometry*

169 To monitor the photophysiology of *F. cylindrus* during the freezing and melting
170 processes, variable chlorophyll *a* fluorescence (ChlF) measurements were conducted
171 using a bench-top Fast Repetition Rate fluorometer (FRRf) (FastOcean Act2Run
172 Systems, Chelsea Technologies) with Act2Run software (Chelsea Technologies).
173 Thawed ice samples were buffered with filtered seawater (ice:seawater ratio = 1: 1) at

174 2.5 °C in the dark for 30 min, and the slushy melted ice samples were placed in a quartz
175 cuvette to measure fluorescence. A single turnover protocol was applied for ChlF
176 measurement; 100 flashlets with 1 μs duration at a wavelength 450 nm and 2 μs
177 intervals for excitation of reaction centres of PSII and 20 flashlets with 1 μs duration
178 and 20 flashlets with 1 μs duration and 100 μs intervals for relaxation. Eighteen light
179 steps were applied to generate a rapid light curve (RLC) from 0 to 800 μmol photons
180 m⁻² s⁻¹, taking <5 min to complete one RLC. At each light step (~15 s), at least five
181 induction and relaxation curves were averaged to obtain ChlF yields, described in Table
182 1, after calibrating the ChlF yields with filtered seawater. According to the models
183 proposed by Kolber et al. (1998), photosynthetic parameters of chlorophyll *a* (chl *a*)
184 induction curves were calculated based on the ChlF yields as shown in Table 1. Electron
185 transport rate through the reaction centres of PSII (RCII) (ETR_{RCII}) was calculated as
186 follows:

188
$$\text{ETR}_{\text{RCII}} = E \times \sigma_{\text{PSII}} \times \frac{F'_q/F'_m}{F_v/F_m} \times \Phi_{\text{RCII}} \times 6.022 \times 10^{-1}$$

187

189 following Suggett et al. (2011) and Schuback et al. (2016), an alternative approach to
190 calculating ETR_{RCII} of Kolber et al. (1998), wherein Φ_{RCII} is the quantum yield of RCII

191 assumed as 1, and the following number is a conversion factor to mol quanta mol
192 $\text{RCII}^{-1} \text{ s}^{-1}$. The calculated ETR_{RCII} at each light step were fitted to the model of Platt et
193 al. (1980) to obtain photosynthesis–irradiance ($\text{ETR}_{\text{RCII}}-E$) parameters (Table 1). To
194 assess the heat dissipation of algal cells, non-photochemical quenching based on the
195 normalized Stern-Volmer (S-V) coefficient (NPQ_{NSV}') under the actinic light equivalent
196 to the incubation light intensities was also calculated following McKew et al. (2013):

197
$$\text{NPQ}_{\text{NSV}}' = F_o' / F_v'$$

198

199 where F_o' is a minimum ChlF yield after a relaxation sequence calculated following
200 Oxborough and Baker (1997) (Table 1).

201

202 *Validation experiments of melting procedures of ice samples for ChlF measurement*

203 While ChlF has been widely used on seawater samples (e.g., Suggett et al. 2011), it
204 has not been broadly applied to ice algae research (Miller et al. 2015) because of the
205 need for the ice samples to be melted. Melting the ice samples changes the
206 photophysiology of the algal cells (e.g., Garrison and Buck 1986, Mikkelsen and
207 Witkowski 2010, Rintala et al. 2014, Campbell et al. 2019). Here, multiple comparisons

208 were conducted on melt procedures of an ice sample from the ice tank. Measurements
209 of ChlF were performed on three treatments of ice samples; (1) intact ice, (2) slushy
210 melted ice suspended in filtered seawater (ice: seawater ratio=1: 1), (3) slowly (24 h)
211 and directly melted samples. The blank calibration for F_o was conducted with filtered
212 seawater as described, however, an empty quartz tube was used for the calibration
213 because it was impossible to prepare a blank ice sample for the treatment 1. It was thus
214 assumed that the ice samples for the treatment had a high enough biomass without F_o
215 calibration. All samples were stored or melted in the dark for 30 min for the treatments
216 1 and 2, whereas the other samples (i.e. the treatment 3) were kept at 2.5 °C during the
217 overnight melting. The FRRf was used for the ice samples from the ice tank as
218 described above.

219

220 *Cell abundance of ice algae*

221 Triplicated microscopic samples were fixed with neutralized formaldehyde solution
222 (final concentration 2%). Cell abundance of *F. cylindrus* was determined with an
223 inverted microscope (Axiovert 25, Zeiss) and a Sedwick-Rafter counting chamber
224 (Pysen-SGI Lmd.). At least 500 cells were enumerated to determine cell abundance
225 (LeGresley and McDermott 2010). Growth rate was calculated following Wood et al.

226 (2005):

228
$$\mu = \frac{\ln(N_t/N_0)}{t - t_0}$$

227

229 *Pigment composition*

230 Pigment concentrations were determined to quantify chlorophylls, photosynthetic and
231 photoprotective carotenoids, and chlorophyll derivatives with a Ultra-High Performance
232 Liquid Chromatography (UHPLC) (Suzuki et al. 2015). On each sampling day,
233 triplicated ice or seawater samples were filtered onto 25 mm GF/F filters (Whatman)
234 using gentle vacuum (<0.013MPa) via a 25 mm polypropylene in-line filter holder
235 (Swinnex, Merck). Rintala et al. (2014) confirmed that fast and direct melting was a
236 reliable method for pigment analysis in ice algae. The filter was flash frozen in liquid
237 nitrogen and stored in a deep freezer (-80 °C). After thawing, the filter was blotted dry
238 with a filter paper, and the pigments were extracted using the *N, N*-dimethylformamide
239 (DMF) bead-beating method (Suzuki et al. 2015). The extracted pigments were
240 suspended in DMF and then injected into an UHPLC for pigment determination. The
241 ratio of diadinoxanthin (DD) and diatoxanthin (DT) was calculated to assess the
242 xanthophyll epoxidation-de-epoxidation cycle and photoprotective strategies of algae
243 (Katayama et al. 2017), assessed as a de-epoxidation state (DES; DT/(DD+DT)). Total

244 chl *a* (Tchl *a*: sum of chl *a*, chlorophyllide *a*, chl *a*-allomer, and chl *a*-epimer)
245 concentrations were calculated as an indicator of algal biomass. Contributions of
246 chlorophyllide (chlide *a*) to Tchl *a* were also calculated as an index of the breakdown
247 of chl *a*. Following Schuback et al. (2016) and Yan et al. (2019), ratios of
248 photoprotective carotenoids (PPC: DD, DT, and β,β -carotene) to photosynthetic
249 carotenoids (PSC: only fucoxanthin here) in diatoms and the xanthophyll pool size
250 $((DD+DT)/Tchl\ a)$ were calculated to quantify photoprotective potentials of the diatom
251 *F. cylindrus*.

252

253 *Gene expression of photosynthesis-related genes; psbA and rbcL*

254 To investigate the mechanisms of freezing and melting stress on cells of *F. cylindrus*
255 in water and in the ice, gene expression of the photosynthesis-related genes, *psbA* and
256 *rbcL*, was measured. To stabilize the RNA, 250 μ L of RNAlater (Sigma) was
257 immediately added to the ice core after collection. Triplicated melted ice and seawater
258 samples were filtered onto two 25 mm, 2 μ m polycarbonate Isopore membrane filters
259 (Millipore) with gentle vacuum (<0.013 MPa) passing through a 25 mm polypropylene
260 in-line filter holder (Swinnex, Merck) for DNA and RNA samples. The DNA samples
261 were placed in a cryotube and flash frozen in liquid nitrogen and stored at -80 °C. RNA

262 samples were suspended in 600 μ L RLT buffer (Qiagen) in a cryotube, to which 10 μ L
263 of β -mercaptoethanol (Sigma-Aldrich) was added. The RNA sample then was flash
264 frozen in liquid nitrogen prior to storage at -80 $^{\circ}$ C until further analysis. DNA and RNA
265 were extracted following Endo et al. (2013) and Endo et al. (2015), respectively. The
266 extracted RNA was reverse-transcribed to complementary DNA (cDNA) with the
267 PrimeScriptTM RT Master Mix (RR036, Takara) reagent according to the
268 manufacturer's specification. DNA and cDNA copy numbers of the *psbA* and *rbcL*
269 genes were quantified by quantitative PCR (qPCR). The primer sets and PCR conditions
270 used in this study are shown in Table S1 in the Supporting Information. Gene
271 expression was defined as the ratio of copy numbers of cDNA to DNA.

272

273 *Statistical analysis*

274 Statistical analyses were conducted using the SigmaPlot software program ver. 11.0
275 (SystStat Software, Inc.). One-way ANOVA with Tukey's test was performed on the
276 individual sampling days in each light treatment to identify variations in ChlF
277 parameters, pigment concentrations and gene expression. The differences in each
278 parameter were considered significant when $p < 0.05$. Two-way ANOVA with Tukey's

279 tests was performed on the individual sampling days and light treatment to identify the
280 differences in ChlF and pigment data to assess the effects of differences in
281 photosynthetic ability and pigment composition between light treatments. Data was
282 transformed for normalization prior to the ANOVA tests with the R statistical software
283 using the R package MASS. Normality and variance of the data were checked by
284 performing Shapiro-Wilk's test and Levene's test using the SigmaPlot software
285 program after the data transformation, respectively.

286

287 RESULTS

288 *Ice physics and ice algal growth*

289 During the experiments, ice thickness remained stable at 5.5 cm with little basal
290 melting or sublimation. Temperature within the ice increased with depth (ice surface:
291 $-22.5\text{ }^{\circ}\text{C}$, ice-water interface: $-2.2\text{ }^{\circ}\text{C}$) (Fig. 2) and the underlying seawater was stable
292 at ca. $-1.8\text{ }^{\circ}\text{C}$ throughout the incubations. Brine salinity decreased with depth from
293 293.7 ± 0.0 to 39.4 ± 0.5 , whereas the brine fraction increased ($3.7 \pm 0.0\%$ to $34 \pm 0\%$,
294 assuming no gas bubbles were present). Nutrient concentrations did not significantly
295 change during the incubations (data not shown). The ice formation concentrated *F.*
296 *cylindrus* cells in the ice (HL: $8883 \pm 224\text{ cells mL}^{-1}$; LL: $8600 \pm 573\text{ cells mL}^{-1}$)

297 compared with under-ice seawater (3551 ± 95 cells mL^{-1} ; LL: 3639 ± 135 cells mL^{-1}).
298 Cells of *F. cylindrus* were thus successfully incorporated into the ice matrix where slow
299 but positive growth in both treatments was observed (0.020 ± 0.001 and 0.020 ± 0.002
300 under HL and LL, respectively); there was no significant difference in growth rate
301 between the treatments ($t=0.00$, $p>0.05$, Welch's *t*-test).

302

303 *Variable chl a fluorescence*

304 *Dark values (F_v/F_m and σ_{PSII})*

305 At the beginning of the incubations (day -05), initial F_v/F_m of *F. cylindrus* showed
306 comparable and relatively high values in both high light (HL: 0.47 ± 0.05) and low light
307 (LL: 0.45 ± 0.06) conditions ($t=0.63$, $p>0.05$, Welch's *t*-test) (Fig. 3A, B). Upon
308 freezing in (day 00), F_v/F_m decreased significantly to 0.2–0.3 in both HL and LL (HL:
309 $F_{(7,40)}=143.27$, $q=31.26$, $p<0.001$; LL; $F_{(7,40)}= 501.93$ $q=35.77$, $p<0.001$, one-way
310 ANOVA, Tukey's test) (Fig. 3A, B), while σ_{PSII} did not change (HL: $F_{(7,40)}=10.59$,
311 $q=2.01$, $p>0.05$; LL: $F_{(7,40)}= 12.97$, $q=3.65$, $p>0.05$, one-way ANOVA) (Fig. 3C, D).
312 Once incorporated into the ice matrix the F_v/F_m of *F. cylindrus* cells remained stable
313 from day 00 to day 20 regardless of the light availability (HL: 0.20 ± 0.03 ; LL: $0.16 \pm$
314 0.05 , $t=1.68$, $p>0.05$, Welch's *t*-test), until initiation of the melt cycle. The lowest F_v/F_m

315 was observed on day 15 in both HL and LL (HL: 0.18 ± 0.02 ; LL: 0.09 ± 0.02) (Fig.
316 3A, B). The σ_{PSII} values at both light levels were relatively stable throughout the
317 incubations with slight decreases with time (Fig. 3C, D). Once the ice had melted,
318 F_v/F_m values seemed to be recovered from the values at day 20 in LL (HL: 0.18 ± 0.02 ;
319 LL: 0.19 ± 0.02) to almost equivalent levels on day -05 (see above), respectively. There
320 were, however, significant differences in F_v/F_m values between day -05 and melt
321 samples both in HL and LL (HL: $q=35.57, p<0.001$; $q=35.77, p<0.001$, one-way
322 ANOVA, Tukey's test) ($39 \pm 1\%$ lower and $15 \pm 1\%$ higher, respectively) (Fig. 3A, B).
323 The responses of σ_{PSII} differed to F_v/F_m , which was significantly different on day -05,
324 but similar to σ_{PSII} values on day 20 regardless of the light availability (HL: $q=1.07$,
325 $p>0.05$; LL: $q=1.08, p>0.05$, one-way ANOVA) (Fig. 3C, D). Immediately after light
326 exposing the melted samples at $800 \mu\text{mol photons m}^{-2} \text{s}^{-1}$, F_v/F_m significantly
327 decreased in both light treatments (HL: $q=13.09, p<0.001$; LL: $q=53.11, p<0.001$, one-
328 way ANOVA, Tukey's test) ($39 \pm 3\%$ and $29 \pm 2\%$ for HL and LL treatments,
329 respectively). Despite the large decreases in F_v/F_m , σ_{PSII} showed minimal variation.

330

331 *Non-photochemical quenching (NPQ_{NSV}')*

332 Values of non-photochemical quenching (NPQ_{NSV}') in both light treatments were low

333 on day -05 prior to freezing in. Upon ice incorporation, NPQ_{NSV} ' significantly
334 increased in both HL and LL treatments (HL: $F_{(7,40)} = 52.55$, $q=44.54$, $p<0.001$; LL:
335 $F_{(7,40)} = 149.81$, $q=10.10$, $p<0.001$, one-way ANOVA, Tukey's test) (Fig. 4). NPQ_{NSV} '
336 in HL plateaued immediately after ice formation (i.e., day 00), while NPQ_{NSV} ' in LL
337 was observed to gradually increase and reach a maximum on day 05 (Fig. 4). Post ice
338 melt, NPQ_{NSV} ' in the LL tank decreased to the identical levels as those observed on day
339 -05 ($q=1.36$, $p>0.05$, one-way ANOVA), whereas the HL treatment showed a
340 significant increase in NPQ_{NSV} ' ($q=6.676$, $p<0.001$, one-way ANOVA, Tukey's test).
341 The light exposure after the melting event significantly enhanced NPQ_{NSV} ' (almost
342 doubled) in both HL and LL treatments (HL: $q=11.39$, $p<0.001$; LL: $q=5.22$, $p=0.012$,
343 one-way ANOVA) (Fig. 4).

344

345 *Photosynthesis-irradiance (ETR_{RCII-E}) curve*

346 The initial slopes of ETR_{RCII-E} curve, α (regarded as light utilization efficiency),
347 dropped significantly when the algae were frozen into the ice (HL: $F_{(7,40)} = 8.20$, $q=6.84$,
348 $p<0.001$; LL: $F_{(7,40)} = 11.27$, $q=8.24$, $p<0.001$, one-way ANOVA, Tukey's test) but did
349 not significantly differ thereafter in HL treatment ($p>0.05$, one-way ANOVA) (Fig. 5A,
350 B). A similar trend was observed in the LL treatment, although α increased significantly

351 towards the end of the incubation ($p < 0.05$, one-way ANOVA, Tukey's test). After the
352 ice melted, α values did not significantly change in HL ($q = 0.97$, $p > 0.05$, one-way
353 ANOVA), while, in LL, α returned the initial levels at day -05. Maximum electron
354 transport rates (ETR_{\max}) in both treatments significantly decreased upon freezing in
355 (HL: $F_{(7,40)} = 7.63$, $q = 11.85$, $p < 0.001$; LL: $F_{(7,40)} = 86.30$, $q = 18.52$, $p < 0.001$, one-way
356 ANOVA, Tukey's test) (from 281 ± 37 and 300 ± 67 to 111 ± 53 and 38 ± 13 in HL and
357 LL treatments, respectively). Upon melting out, ETR_{\max} in LL returned (335 ± 57) to
358 the initial levels at day -05 ($q = 2.40$, $p > 0.05$, one-way ANOVA), whereas, in HL,
359 ETR_{\max} was not recovered ($q = 14.41$, $p < 0.001$, one-way ANOVA, Tukey's test) (Fig.
360 5C, D). Light saturation indices, E_k , gradually decreased during the course of the
361 incubation experiments without any conspicuous variation during the frozen period
362 (Fig. 5E, F). The HL treatment showed higher E_k throughout the frozen period from day
363 05 to day 20 compared to LL ($F_{(1,40)} = 9.02$, $p = 0.004$, two-way ANOVA, Tukey's test).
364 When melted out, E_k values returned to the initial levels on day -05 in both treatments
365 although the LL treatment show a higher E_k (HL: $F_{(7,40)} = 7.63$, $q = 0.63$, $p > 0.05$; LL:
366 $F_{(7,40)} = 66.51$, $q = 12.30$, $p < 0.001$, one-way ANOVA, Tukey's test). On the other hand,
367 E_k significantly decreased in both HL and LL treatments (HL: $q = 8.20$, $p < 0.001$; LL:
368 $q = 7.91$, $p < 0.001$, one-way ANOVA, Tukey's test) (Fig. 5E, F).

369

370 *Validation experiments for sample melt procedures*

371 Variable ChlF parameters varied among the different melt procedures of the ice sample
372 (Fig. S2 in the Supporting Information). When the intact crushed ice sample was packed
373 directly into a quartz tube, F_v/F_m values were lower, followed by that of the slushy
374 melted sample. These values were almost the same and did not show any significant
375 difference ($F_{(2,7)}=10.76$, $q=2.90$, $p>0.05$, one-way ANOVA), whereas the slow-direct
376 melt sample showed a significantly higher value compared to its counterparts ($q=4.94$,
377 $p=0.024$, one-way ANOVA, Tukey's test). Unlike F_v/F_m values, σ_{PSII} varied little
378 regardless of the melt methods and did not show any significant enhancement or
379 suppression ($F_{(2,7)}=3.31$, $p>0.05$, one-way ANOVA) (Fig. S2 in the Supporting
380 Information).

381

382 *Pigment composition*

383 Initial Tchl *a* concentrations were at the same level between incubations at day-05
384 ($F_{(1,31)}=2.29$, $p>0.05$, Two-way ANOVA) (Fig. 6A, B). After *F. cylindrus* cells were
385 incorporated into the ice, ice algae in the HL treatment maintained stable Tchl *a*
386 biomass ($F_{(7,16)}=2.27$, $q=0.09$, $p>0.05$, one-way ANOVA) although Tchl *a* in the LL

387 treatment showed a gradual increase. Contributions of chl *a* to Tchl *a* were slightly
388 higher in the HL treatment than in the LL tank throughout the incubations
389 ($F_{(1,31)}=59.96$, $p<0.001$, Two-way ANOVA, Tukey's test; 48.0–62.5% and 34.0–54.9%,
390 respectively) (Fig. 6A, B). The cellular DD-DT pool size in both the HL and LL
391 treatments at the beginning of the incubations was comparable ($F_{(1,31)}=73.27$, $q=1.76$,
392 $p>0.05$, Two-way ANOVA), whereas, during the frozen period the cellular pool size
393 grew faster was significantly larger in the HL ice tank than those in the LL tank
394 ($F_{(7,16)}=73.27$, $q=12.11$, $p<0.001$, Two-way ANOVA, Tukey's test; 17.3–25.3% and
395 8.8–14.7% to Tchl *a*, respectively) (Fig. 6C, D). During the frozen period from day 05
396 to day 20, DES was also higher in the HL ice tank (0.293–0.552) compared to the LL
397 ice tank (0.107–0.231) ($F_{(1,31)}=35.65$, $p=0.027$, Two-way ANOVA, Tukey's test) (Fig.
398 6C, D). Light exposure enhanced the DES in both treatments (4.20- and 5.23-fold
399 increases in the HL and LL ice tank, respectively). Higher PPC/PSC ratios were present
400 in the HL ice tank than in LL throughout the incubations ($F_{(1,31)}=69.22$, $p<0.001$, Two-
401 way ANOVA, Tukey's test) (Fig. 6E, F). The PPC/PSC ratios showed little variation
402 before and after light exposure in both light treatments (HL: $F_{(7,16)}=3.82$, $q=0.04$,
403 $p>0.05$; LL: $F_{(7,16)}=3.86$, $q=0.85$, $p>0.05$, one-way ANOVA).

404

405 *Gene expression of photosynthesis-related genes*

406 *rbcL*

407 Prior to incubation there was no significant difference in the expression of the *rbcL*
408 gene in either HL or LL ($t=0.33$, $p>0.05$, Welch's *t*-test) (Fig. 7A, B). Transcriptional
409 activity of the *rbcL* gene was highly upregulated when algae were frozen into the ice
410 (HL: $F_{(7,16)}=7.65$, $q=5.30$, $p=0.03$; LL: $F_{(7,16)}=7.39$, $q=6.89$, $p=0.003$, one-way
411 ANOVA, Tukey's test) in both HL and LL (Fig. 7A, B). After day 05 and day 10, gene
412 expression of the *rbcL* gene decreased significantly in the HL and LL treatments (HL:
413 $q=7.290$, $p=0.002$; LL: $q=6.79$ $p=0.040$, one-way ANOVA, Tukey's test), respectively
414 (Fig. 7A, B). This low level was sustained during the frozen period. Comparing the
415 results of melt and light periods, the *rbcL* gene expression did not show any
416 conspicuous change in either treatment (HL: $q=2.173$, $p>0.05$; LL: $q=0.31$, $p>0.05$,
417 one-way ANOVA).

418

419 *psbA*

420 Unlike the *rbcL* gene, the expression of the *psbA* gene differed with respect to light
421 availability (Fig. 7C, D). The initial value in the HL treatment was ~2-fold higher than
422 that in LL. In HL, transcription of the *psbA* gene was highly upregulated during freezing

423 ($F_{(7,16)}=19.90$, $q=10.28$, $p<0.001$, one-way ANOVA, Tukey's test); which was similar
424 to the *rbcL* gene. In LL, upregulation of *psbA* was not evident ($F_{(7,16)}=2.02$, $p>0.05$,
425 one-way ANOVA). Expression of *psbA* in HL showed a similar trend to the *rbcL* gene,
426 whereas, under LL, the *psbA* gene expression did not change throughout the experiment
427 (Fig. 7C, D).

428

429 DISCUSSION

430 *Ice tank incubation*

431 We here, for the first time, successfully demonstrated the use of a purpose designed ice
432 tank to study the photophysiology of ice algae for a prolonged period (i.e. 20 days)
433 under environmentally relevant conditions. When ice formed, cooling of the water body
434 from the surface in the ice tank, in a -20 °C freezer, realistically mimicked *in situ* ice
435 formation events in wintertime, with cells of *F. cylindrus* successfully incorporated into
436 the ice. The temperature profile of the artificial sea ice indicates that the ice properties
437 simulated winter ice environments, inferred from a sharp decrease in temperature with
438 depth (Fig. 2) (Petrich and Eicken 2017). It suggests that the ice tank was well suited to
439 investigate survival strategies of ice algae under chronic multiple stress in wintertime.

440 The identical initial F_v/F_m values at day-05 (Fig. 3A, B) indicate that the two discrete
441 ice tank runs (i.e. HL and LL treatments) started with the similar physiological states of
442 *F. cylindrus*.

443

444 *Freezing event*

445 The freezing events in the ice tank experiments reported herein suppressed
446 photochemical quantum efficiency of PSII (Fig. 3A, B). Drawdowns in F_v/F_m were also
447 observed in the previous ice tank study using *Phaeocystis antarctica* (Kennedy et al.
448 2012) during ice formation. This suppression has also been noted in natural sea ice,
449 inferred from lower F_v/F_m of ice algae than pelagic phytoplankton (McMinn et al.
450 2008, Yamamoto et al. 2014).

451 A significant amount of chl *a* breakdown products has been reported in ice algae of
452 both landfast and pack-ice in the Arctic and Antarctic (e.g., Horner 1985, Alou-Font et
453 al. 2013). One might interpret the here observed increase in chl *a* (Fig. 6A, B) as
454 inactivation of PSII reaction centres. Chl *a*, lacking the phytol chain, has a less
455 pigment aggregation potential (Fiedor et al. 2003), leading to reduced coupling of
456 excitons (inefficient energy transfer between pigments) (Rosenbach-Belkin et al. 1991).

457 However, the stable amount of chl *a* during the freezing events (Fig. 6A, B)
458 indicates that the existence of chl *a* had only a minor effect on the drawdown in
459 F_v/F_m . Also, not all inactive pigments (i.e. chl *a*) are involved in reaction centres
460 but function as photosynthetic antennae pigments.

461 Suggett et al. (2009) demonstrated that chronic stress decreases F_v/F_m with a
462 concomitant enhancement of σ_{PSII} because of the absorbed light energy being funnelled
463 to fewer active PSII reaction centres if some reaction centres are damaged/inactive
464 (Suggett et al. 2009, 2011, Falkowski and Raven 2013). In this study, however, little
465 variation in σ_{PSII} was observed during the freezing event (Fig. 3C, D). This suggests that
466 photoinactivation could not be significant during ice formation.

467 Freezing stress, combined with low temperatures and high brine salinity, could be the
468 main cause of the reduction in the photochemistry of PSII and the capacity of electron
469 sinks (Ensminger et al. 2006, Ralph et al. 2007). Low temperatures reduce membrane
470 viscosity, which suppresses photochemical reactions in the electron transport chain
471 (Morgan-Kiss et al. 2006). At the same time, high brine salinity might suppress the
472 reduction capability of electron donors around PSII (i.e., the first quinone electron
473 acceptor Q_A and the plastoquinone (PQ) pool; Ralph et al. 2007). Indeed, the here

474 observed high brine salinity (55 on average and >80 in the upper part of the ice) was
475 high enough to suppress the downstream components of PSII (Ralph et al. 2007). This
476 combined stress of low temperature and high salinity has been found to stagnate
477 electron transfer along the electron transport chain down to ferredoxin and cause
478 “electron clogging” (e.g., Lazár et al. 2005). This “electron clogging” consequently can
479 lead to (a) the low F_v/F_m (e.g., Schwarz et al. 2017), (b) overreduction of the PQ pool
480 (Maxwell et al. 1995, Allen and Nilson 1997, Pfannschmidt 2003) and (c) an imbalance
481 of the photochemical electron transport (“photostasis”; Öquist and Huner 2003). We
482 interpret the here observed increase in NPQ_{NSV} (Fig. 4) as a measure for alleviating
483 excess excitation pressure (e.g. Caron et al. 1987, Ting and Owens 1993, Goss and
484 Jakob 2010).

485 The HL treatment exhibited a larger DD-DT pool and higher PPC/PSC compared with
486 the LL counterpart (Fig. 6C, D, E, F). These light responses can be interpreted as up-
487 front protection to mitigate the production of reactive oxygen species under high light
488 (McMinn and Hegseth 2004, Katayama and Taguchi 2013, Kuczynska et al. 2015). This
489 notion is supported by field observations of (Kropuenske et al. 2009, Schuback et al.
490 2016, Galindo et al. 2017) and emphasized light-photoprotection relationships (Lavaud
491 et al. 2002, Domingues et al. 2012).

492 Photosynthetic performance, assessed with $ETR_{RCII}-E$ curves, showed rapid
493 photoacclimation responses during freezing; a greater decrease in ETR_{max} than that of α
494 led to apparent dark acclimation with a lower E_k after freezing (Fig. 5). However, the
495 concomitant decrease of α does not coincide with classical shade photoacclimatisation
496 strategies (i.e. higher α and lower E_k under lower light would be expected; MacIntyre et
497 al. 2002). The decrease in α suggests a decrease in n_{PSII} , the active fraction of PSII to
498 chl *a* (e.g. Falkowski and Raven 2013). Values of α are represented as a product of σ_{PSII}
499 and n_{PSII} ; however, σ_{PSII} values were stable during the freezing event, suggesting
500 photoinactivation of RCII (i.e., lowered n_{PSII}). It is thus suggested that both the
501 combination of direct photoinactivation and electron clogging deactivated the
502 photochemical reactions at RCII. The freezing event, therefore, suppressed RCII
503 photochemistry both directly and indirectly.

504 The strong upregulation of expression of the *psbA* gene in the HL treatment
505 accelerated repair of damaged PSII under overexcitation pressure in the HL condition
506 and vice versa (Fig. 7C, D) (Petrou et al. 2010, Galindo et al. 2017). The significant
507 upregulation of the *rbcL* gene (Fig. 7A, B) could be evidence of a cold acclimation
508 strategy to increase cellular RuBisCO and compensate for the low catalytic activity of
509 the temperature-sensitive enzyme by increasing its concentration (Devos et al. 1998,

510 Lyon and Mock 2014, Young et al. 2015). However, Mock and Hoch (2005) reported
511 downregulation of *rbcL* transcription in *F. cylindrus* under low temperatures.
512
513 *During the frozen period*
514 ChlF parameters remained relatively stable during the frozen period and little variation
515 in F_v/F_m , σ_{PSII} , and NPQ_{NSV} values were observed within the ice (Figs. 3 and 4),
516 indicating that sea ice is a stable platform for algal photosynthesis (Maccario et al.
517 2015, Arrigo 2017). The comparable levels of F_v/F_m and σ_{PSII} in both ice tanks suggest
518 that the *F. cylindrus* cells sustained or optimized their photosynthesis within the ice
519 regardless of light availability (Fig. 3). This physiological acclimation to ice
520 environments may play a key role in the successful survival and proliferation of ice
521 algae within and at the bottom of sea ice (Kropuenske et al. 2010, Lacour et al. 2018).
522 McMinn and Hegseth (2004) suggested that ice diatoms can grow out in sea ice if
523 F_v/F_m is >0.125 . In this study, the observed F_v/F_m values during the frozen period were
524 high enough to actively grow in the ice. Indeed, this study, for the first time, reported
525 positive growth in the ice tank. Although the growth rates in both treatments ($\sim 0.02\text{ d}^{-1}$)
526 were lower than other reported values from culture experiments (e.g., Mock and Hoch
527 2008, Kropuenske et al. 2010). Interestingly, the growth rates in both the HL and LL

528 treatments were comparable regardless of the under-ice light intensities. This indicates
529 that light availability was not a limiting factor for algal growth in the artificial sea ice.
530 Evidently, photosynthetic and photoprotective abilities between the HL and LL ice
531 tanks were comparable during the frozen periods, as inferred from the identical levels of
532 F_v/F_m and NPQ_{NSV} (Fig. 3A, B; Fig. 4). As discussed above, the electron clogging
533 caused by multiple co-stressors could be the major determinant of algal growth. The
534 low temperature lowered the enzymatic activity of RuBisCO (Young et al. 2015), which
535 could be another possible cause of the identical growth rates observed in both HL and
536 LL treatments. The gradual increase in light utilization index α in the LL ice tank (Fig.
537 5A, B) was consistent with the classical concept of photoacclimation (MacIntyre et al.
538 2002). As noted above, σ_{PSII} was stable in the LL treatment (Fig. 3C, D). Cells under
539 LL may increase the proportion of active RCII relative to pigmentation (chl *a*) in order
540 to enhance light capture during freezing in (Fig. 5E, F). Only algae in the LL ice tank
541 showed a gradual increase in Tchl *a* concentration, in spite of the same algal growth rate
542 in both HL and LL treatments; this could be further evidence of dark acclimation (e.g.,
543 Falkowski and Owens 1980). The smaller PPC/PSC in the LL ice tank also supports this
544 suggestion by indicating preferential synthesis of photosynthetic chlorophylls and
545 carotenoids rather than PPC (Fig. 6E, F). Cells in the HL treatment strengthened their

546 photoprotective capability, reflected in higher values of PPC/PSC and DES compared to
547 cells in LL (Fig. 6C, D, E, F) (Kropuenske et al. 2009, 2010). However, both HL and
548 LL treatments showed increased their DD-DT pool and DES, suggesting again a highly
549 reduced PQ pool due to the electron clogging (i.e., the development of ΔpH) (Leptit et
550 al. 2010, 2013). Interestingly, NPQ_{NSV} ' levels were comparable between the light
551 treatments regardless of the difference in DES (Figs. 4 and 5C, D). Nymark et al. (2013)
552 suggested that low-light acclimated cells have more *LHCX* proteins, which enlarges
553 their NPQ capacity (Bailleul et al. 2010). Interestingly, the transcriptional activity of the
554 *rbcL* gene greatly decreased after the sharp increase on day 00 (onset of freezing),
555 suggesting that cells had used the high abundance of RuBisCO (or its mRNA) that was
556 synthesized during the freezing event (Fig. 7A, B). The constant but lower expression of
557 *psbA* could keep the repair of PSII to a 'business as usual' rate (Fig. 7C, D), whereas the
558 downregulation of the gene after initial significant upregulation in the HL treatment
559 might be caused to alleviate the photochemical imbalance in the electron transport chain
560 due to the upregulation when shocked by freezing stress (e.g. changes in PSII to PSI
561 ratio).

562

563 *Light exposure after ice melt*

564 Light exposure to released algal cells in spring time suppressed photosynthetic
565 activities. Exposure to irradiance following melting decreased F_v/F_m due to the high
566 excitation pressure (Fig. 3A, B), despite ice melt before light exposure increasing
567 photochemical activity. The increase in F_v/F_m after ice melt was consistent with results
568 of the validation experiments (Fig. S2 in the Supporting Information). The degree of
569 drawdown in F_v/F_m was comparable regardless of the incubation light intensity after
570 light exposure (Fig. 3A, B). NPQ_{NSV} was downregulated when the ice melted but was
571 enhanced after light exposure (Fig. 4). This reverse response to light exposure between
572 F_v/F_m and NPQ_{NSV} might be evidence for fast activation of photoprotection (Figs. 3A,
573 B and 4) especially in the HL treatment with the higher DES (Fig. 6C, D). Damage of
574 PSII, however, was likely because of the considerable increase in the ratio of chl *a*
575 to Tchl *a* after light exposure in both ice tanks (Fig. 6A, B). One might suspect that the
576 melting process prior to sample filtration caused the significant breakdown of chl *a* with
577 activation of chlorophyllase (Jeffery and Hallegraeff 1987); however, a stable level of
578 chl *a* to Tchl *a* observed throughout the incubation period even from day -05 before
579 ice formation (Fig. 5A, B) suggests the melting process (osmotic stress) could not be
580 responsible for the high concentrations of chl *a* and other degraded pigments.
581 However, the significant difference in chl *a* contributions between HL and LL

582 throughout the incubations might relate to the breakdown of chl *a* because high light to
583 *F. cylindrus* leads a high qI (non-photochemical quenching by photoinactivation)
584 (Kropuenske et al. 2009). After ice melt, PPC/PSC decreased while F_v/F_m increased
585 (Figs. 3A, B and 6E, F). This suggests a re-optimization of photosynthetic performance
586 to a water environment after release from freezing stress. Light exposure, however,
587 activated the DD-DT xanthophyll cycle (i.e., de-epoxidation) (Fig. 6C, D) (Petrou et al.
588 2010), although the size of the DD-DT pool was little changed (Fig. 6C, D). Activation
589 of the DD-DT cycle is the fastest photoprotective strategy and occurs at a scale of
590 seconds to minutes (Goss and Jakob 2010), whereas the size of the pool actually
591 changes much slower. Interestingly, NPQ_{NSV}' in the HL treatment was much higher
592 than that of the LL treatment with differences in their DD-DT pool size (Figs. 4 and 6C,
593 D), suggesting that pigmentation and light history were largely responsible for their
594 potential photoprotective ability (Szechyńska- Hebda et al. 2010, Galindo et al. 2017). It
595 seems to be unusual that E_k values significantly decreased (i.e. dark acclimation) upon
596 light exposure, contrary to the expected response from high-light acclimation (Fig. 5E,
597 F). Transcriptional activity of the *psbA* gene was stable in both treatments after light
598 exposure (Fig. 7C, D). It is suggested that algal cells did not immediately start to
599 synthesize mRNA for repair of the damaged RCII, possibly because post-transcriptional

600 regulation is significant for D1 protein synthesis (Malnoë et al. 1988, Danon and
601 Mayfield 1991) with a large mRNA pool (Mulo et al. 2012). The dark reaction might
602 also be independent or to have been slow to respond to the light exposure event because
603 the gene expression of the *rbcL* gene was invariant before and after light exposure (Fig.
604 6A, B).

605

606 CONCLUSIONS

607 This study demonstrates how the combined effects of ice formation and melting
608 together with light exposure affect the photophysiology of *F. cylindrus*. This study is
609 the first attempt to conduct the *ex situ* incubation of the ice algal *F. cylindrus* in
610 artificial sea ice to quantify the effects of multiple co-stressors in sea ice and to provide
611 new insights into the fate of ice algae. The ice tank successfully mimicked ice formation
612 events as experienced in the field (Figs. 1 and 2). This enabled investigation into the
613 effects of multiple co-stressors on the capacity of *F. cylindrus* to survive this ephemeral
614 habitat. We successfully observed, for the first time, positive growth of ice algal cells in
615 artificial sea ice. Ice formation events suppressed the photochemical process of RCII,
616 despite optimal irradiance prior to freezing in (Fig. 3A, B). This was likely a result of
617 high brine salinity and low temperature, which led to electron clogging in the electron

618 transport chain. Ice algal cells rapidly optimized their photophysiology to the dark
619 environment within the ice, inferred from decreases in E_k (Fig. 3 and 5E, F). Light
620 availability could affect the photoacclimative ability of ice algae, possibly by increasing
621 active RCII. Further investigation on the connectivity of photosynthetic antennae to
622 RCII would be needed to address the efficiency of energy transfer to RCII (e.g.,
623 D'Haene et al. 2015, Yoshida et al. 2018). Although ice melt stimulated algal
624 photosynthesis, the subsequent light exposure resulted in photoinhibition (Fig. 3A, B)
625 with significant chl *a* accumulation and NPQ_{NSV}' enhancement. However,
626 photoprotection was rapidly activated. We conclude that the diatom *F. cylindrus*
627 possesses a high photosynthetic plasticity that contributes to the ecological success of
628 this species in both pelagic and sea-ice habitats.

629

630 ACKNOWLEDGEMENTS

631 We greatly appreciate the valuable comments provided by the anonymous reviewers.
632 Thanks to Ms. Akiko Kamimura for her support in pigment analysis. We appreciate
633 Prof. Philip Boyd for providing his benchtop FRRf. This research was partly supported

634 by Australian Antarctic Science Program (AAS4319) and JSPS Grants-in-Aid for
635 Scientific Research (JP18H03352, JP17H00775).

636 **LIST OF TABLE**

637 Table 1. Terminology and definition of chlorophyll *a* fluorescence yields obtained from
638 FRRf fluorometry

639

640 **LIST OF FIGURES**

641 Figure 1. A schematic (A) and a photograph (B) of the 70 L ice tank in a $-20\text{ }^{\circ}\text{C}$ freezer.

642

643 Figure 2. Vertical profiles of ice temperature (T_{ice} ; closed circle), brine salinity (S_{br} :
644 open circle), and the fraction of brine volume (V_{br} : closed square) in artificial sea ice in
645 the ice tank.

646 Error bars indicate 1 standard deviation ($n=3$).

647

648 Figure 3. Maximum photochemical quantum yield of PSII (F_v/F_m) (A and B) and
649 functional absorption cross-section of PSII (σ_{PSII}) (C and D) during the ice tank
650 incubation experiments.

651 Left (A and C) and right (B and D) panels indicate data from the HL and LL treatment,
652 respectively. Open, closed and shaded bars indicate values of seawater samples before
653 freezing, ice and seawater samples after melting, respectively. Different letters above
654 bars in a panel indicate significant differences in values between sampling days with
655 one-way ANOVA with Tukey's test; there is no significant difference between values if
656 a given letter is shown in the combination of letters of the counterparts. The D stands
657 for 'day', while Melt and Light indicate values after melting and light exposure
658 experiments, respectively. Error bars show 1 standard deviation ($n \geq 5$).

659

660 Figure 4. Non-photochemical quenching based on the normalized Stern-Volmer
661 quenching coefficient under the actinic light (150 and $30 \mu\text{mol photons m}^{-2} \text{s}^{-1}$ for HL
662 and LL, respectively) (NPQ_{NSV}) during the ice tank incubation experiments. Panels A
663 and B indicate data from the HL and LL treatments, respectively. Different letters above
664 bars in a panel indicate significant differences in values between sampling days with
665 one-way ANOVA with Tukey's test; there is no significant difference between values if
666 a given letter is shown in the combination of letters of the counterparts. The D stands
667 for 'day', while Melt and Light indicate values after melting and light exposure
668 experiments, respectively. Error bars show 1 standard deviation ($n \geq 5$).

669

670 Figure 5. Photosynthesis–irradiance ($ETR_{RCII}-E$) parameters during the ice tank
671 incubation experiments. Top panels (A and B) show light utilization efficiency under
672 dim light (α) as initial slopes of the $ETR_{RCII}-E$ curves, middle panels (C and D) indicate
673 maximum electron transport rate (ETR_{max}), and bottom panels (E and F) show light
674 saturation index (E_k). Left (A, C and E) and right (B, D, and F) panels show data from
675 the HL and LL treatments. Different letters above bars in a panel indicate significant
676 differences in values between sampling days with one-way ANOVA with Tukey’s test;
677 there is no significant difference between values if a given letter is shown in the
678 combination of letters of the counterparts. The D stands for ‘day’, while Melt and Light
679 indicate values after melting and light exposure experiments, respectively. Error bars
680 show 1 standard deviation ($n \geq 5$).

681

682 Figure 6. Variations in pigment concentrations during the ice tank incubation
683 experiments. Top panels (A and B) show total chl *a* concentration (Tchl *a*) [mg m^{-3}]
684 and contribution of chlorophyllide *a* to Tchl *a*, middle panels (C and D) indicate the size
685 of DD-DT pool ($(DD+DT)/Tchl\ a$) and de-epoxidation state of xanthophyll pigments

686 (DES; DT/(DD+DT)), and bottom panels (E and F) show ratio of photoprotective
687 carotenoids (PPC) to the photosynthetic carotenoid (PSC) quantified with UHPLC. Left
688 (A, C, and E) and right (B, D, and F) show data from the HL and LL treatments,
689 respectively. The D stands for 'day', while Melt and Light indicate values after melting
690 and light exposure experiments, respectively. Results of one-way and two-way ANOVA
691 tests performed on the pigment data were described in the text. Error bars show 1
692 standard deviation ($n=3$).

693

694 Figure 7. Gene expression [cDNA/DNA] of photosynthesis-related genes. Top (A and
695 B) and bottom (C and D) panels show gene expression of the *rbcL* and *psbA* genes
696 during the ice tank incubation experiments. Left (A and C) and right (B and D) show
697 data from the HL and LL treatments, respectively. Different letters above bars in a panel
698 indicate significant differences in values between sampling days with one-way ANOVA
699 with Tukey's test; there is no significant difference between values if a given letter is
700 shown in the combination of letters of the counterparts. The D stands for 'day', while
701 Melt and Light indicate values after melting and light exposure experiments,
702 respectively. Error bars show 1 standard deviation ($n=3$).

703

704 **LIST OF SUPPLEMENTAL MATERIALS**

705 Table S1. Primer sets and PCR conditions of qPCR and qRT-PCR for the *psbA* and

706 *rbcL* genes

707

708 Figure S1. A photo of the ice tank with a light panel.

709 The light panel has a white LED with light diffuser to homogenize the light field over

710 the ice.

711

712 Figure S2. Chlorophyll *a* fluorescence parameters with different melting procedures.

713 (a): Maximum quantum yield of PSII photochemistry (F_v/F_m); (b): functional

714 absorption cross-section (σ_{PSII}), determined with FRR fluorometry.

715 Intact ice: intact ice placed into the cuvette for ChlF measurement; slush; ice sample

716 partially melted in filtered seawater; Direct slow: melted ice sample overnight at 2.5 °C.

717 Different letters indicate significant differences between the given values. Error bars

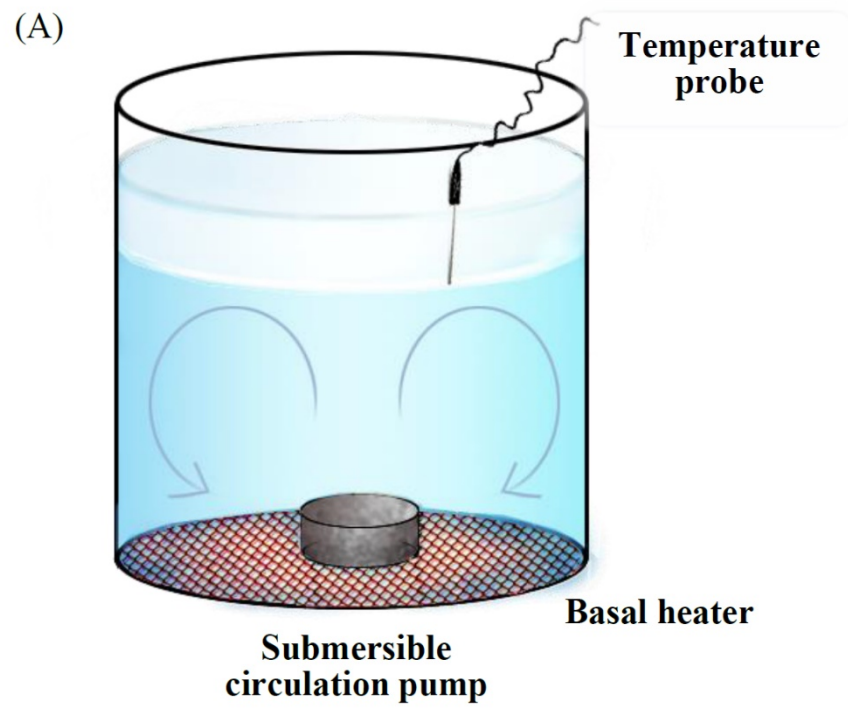
718 indicate 1 standard deviation. $n=6$.

Table 1.

Yield and parameter	Unit	Derivation or reference	
Fluorescence yield			
F	Fluorescence yield	Unitless	
F_o	Minimum fluorescence yield of dark regulated cells	Unitless	
F_m	Maximum fluorescence yield of dark regulated cells	Unitless	
F_v	Maximum variable fluorescence yield	Unitless	$F_m - F_o$
F'	Fluorescence yield under actinic light	Unitless	Oxborough and Baker (1997)
F_o'	Minimum fluorescence yield of actinic light-acclimated cells	Unitless	(1997)
F_m'	Maximum fluorescence yield of actinic light-acclimated cells	Unitless	
F_v'	Variable fluorescence yield under actinic light	Unitless	$F_m' - F_o'$
F_q'	Difference in fluorescence yields between F' and F_m'	Unitless	$F_m' - F'$
Fluorescence parameters in the dark			
σ_{PSII}	Functional absorption cross-section of PSII in the dark	$\text{nm}^2 \text{RCII}^{-1}$	Kolber et al. (1998)
F_v/F_m	Maximum quantum yield of PSII photochemistry	Unitless	$(F_m - F_o)/F_m$
τ	Time constant for Q_A reoxidation	ms	Kolber et al. (1998)
Fluorescence parameters under actinic light			
F_q'/F_m'	Effective photochemical efficiency of PSII under actinic light	Unitless	$(F_m' - F')/F_m'$
NPQ_{NSV}'	Non-photochemical quenching based on the S-V approach	Unitless	McKew et al. (2013)
ETR_{RCII}-E curve parameters			
ETR_{RCII}	Absolute electron transport rate through RCII	$\text{mol e}^{-1} \text{s}^{-1}$	Schuback et al. (2016)
E	Actinic light irradiance	$\text{mol photons m}^{-2} \text{s}^{-1}$	
α	Light utilization index under dim light	$(\text{mol e}^{-1} \text{s}^{-1}) (\mu\text{mol photons m}^{-2} \text{s}^{-1})^{-1}$	Platt et al. (1980)
β	Light inhibition index under high light caused PSII photoinhibition	$(\text{mol e}^{-1} \text{s}^{-1}) (\mu\text{mol photons m}^{-2} \text{s}^{-1})^{-1}$	Platt et al. (1980)
ETR_{max}	Maximum electron transport rate through RCII	$\text{mol e}^{-1} \text{s}^{-1}$	Platt et al. (1980)
E_k	Light saturation index	$\mu\text{mol photons m}^{-2} \text{s}^{-1}$	Platt et al. (1980)

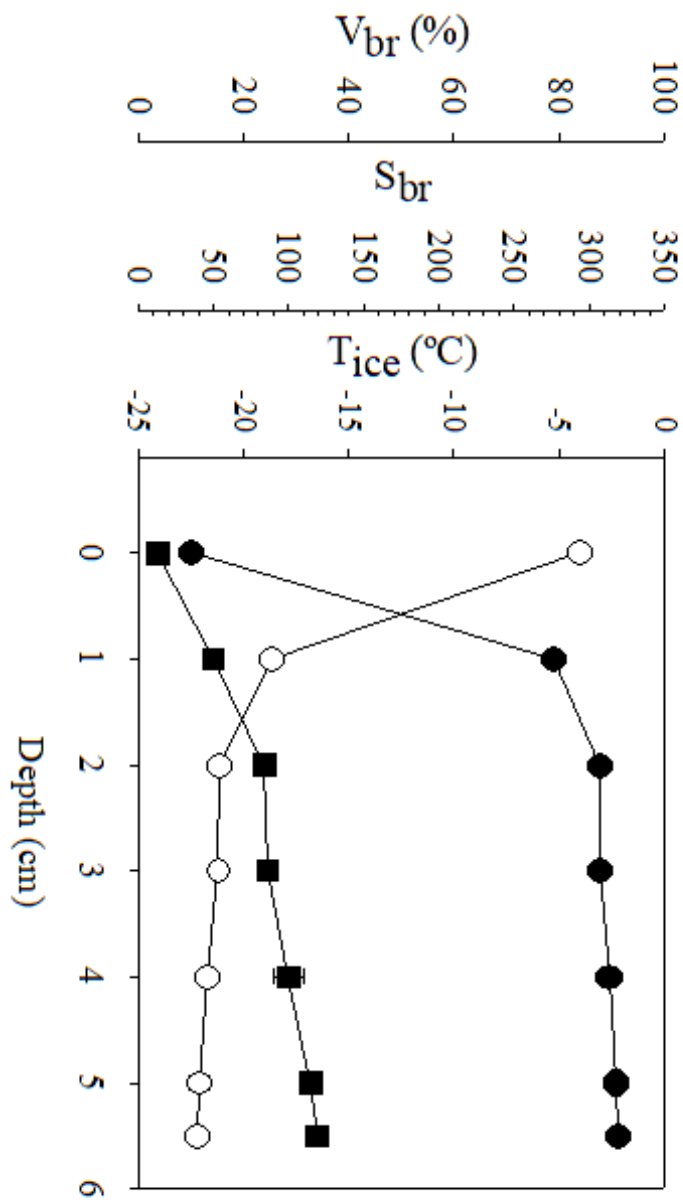
Table S1

<i>psbA</i>	
Forward primer	5'-AGAACCACCAAATACACCAGCAA-3'
Reverse primer	5'-TCCAAGCTGAGCACAACATCTT-3'
Amplicon size	71
PCR condition	94 °C for 60 s; 40 cycles under 98 °C for 10 s, 62 °C for 60 s, and 72 °C for 60s
Baseline gene	Gene fragment of <i>Fragilariopsis cylindrus</i> from Antarctic sea ice ^{*1}
Reference	Krell et al. (2007)
<i>rbcL</i>	
Forward primer	5'-GATGATGARAAAYATTA ACTCW-3'
Reverse primer	5'-TAWGAACCTTTWACTTCWCC-3'
Amplicon size	113
PCR condition	94 °C for 60 s; 40 cycles under 98 °C for 10 s, 55 °C for 60 s, and 72 °C for 60s
Baseline gene	Gene fragment of <i>Thalassiosira weissflogii</i> (CCMP1336)
Reference	John et al. (2007); Endo et al. (2015)
720	*1: The isolate of <i>F.cylindrus</i> was obtained from Antarctic sea ice in the Weddel Sea in 1991
721	(Krell et al., 2007).



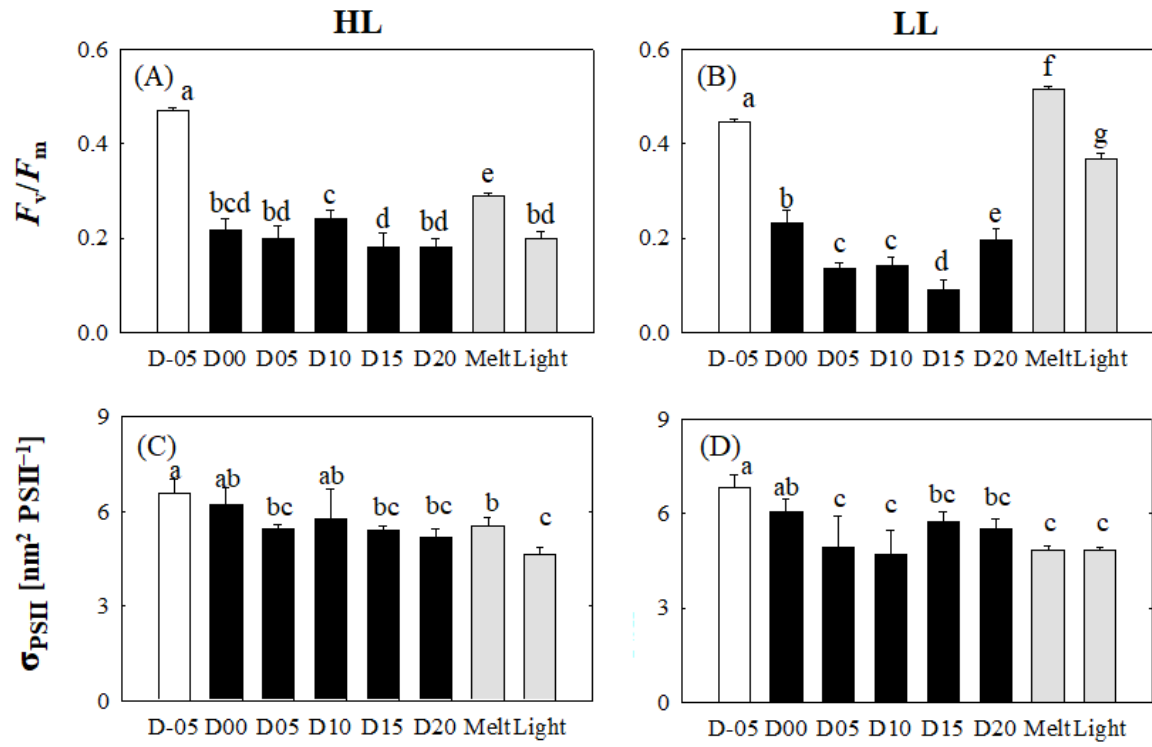
722

723 Fig. 1



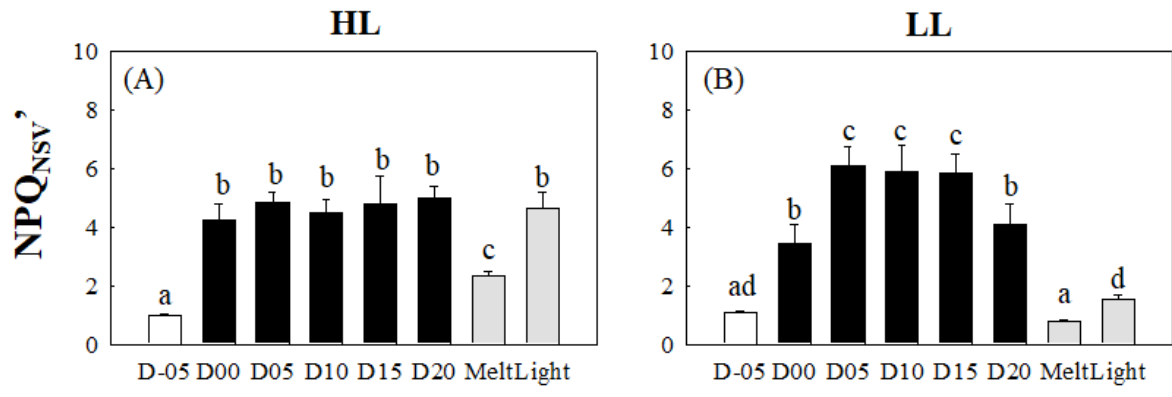
724

725 Fig.2



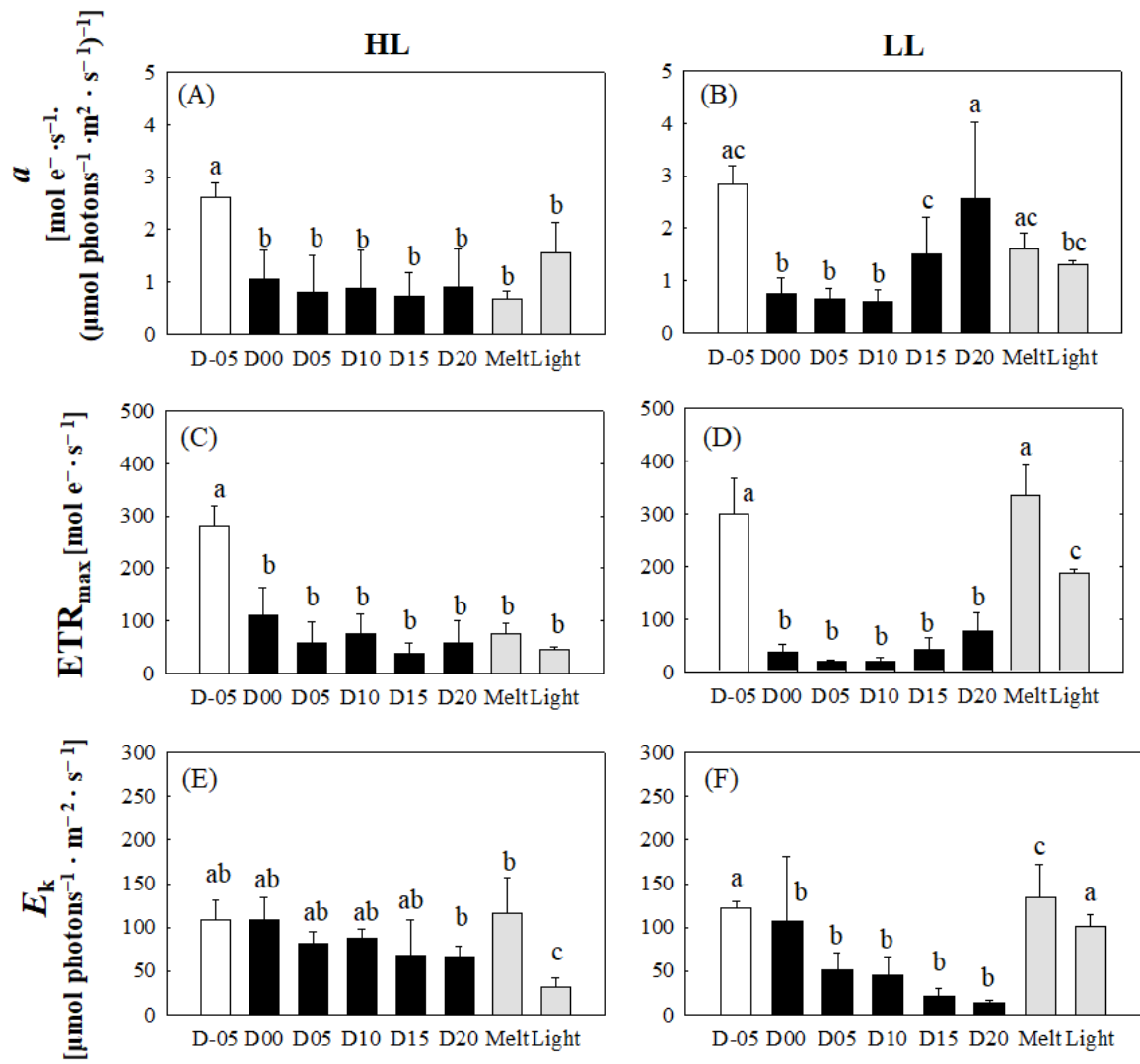
726

727 Fig. 3



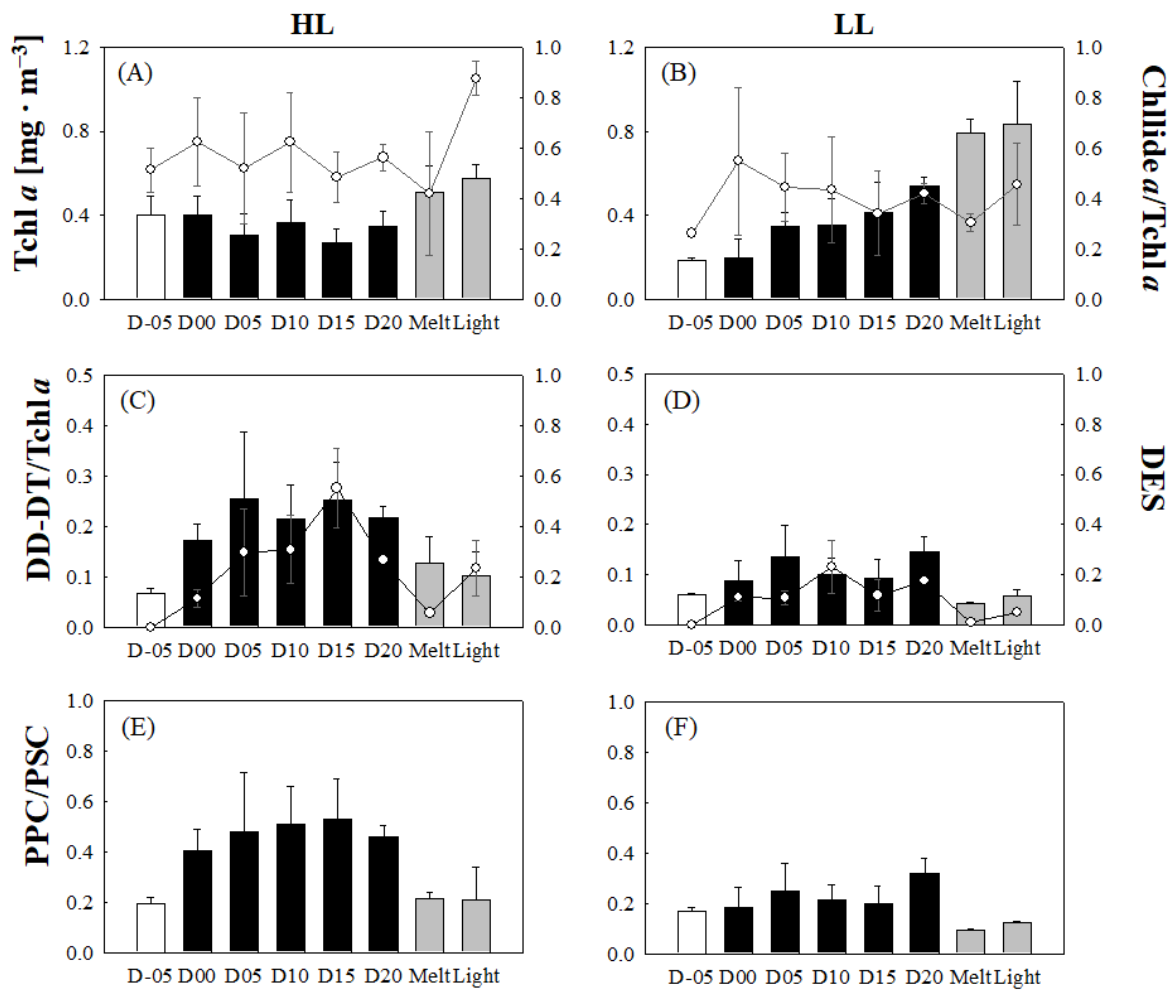
728

729 Fig. 4



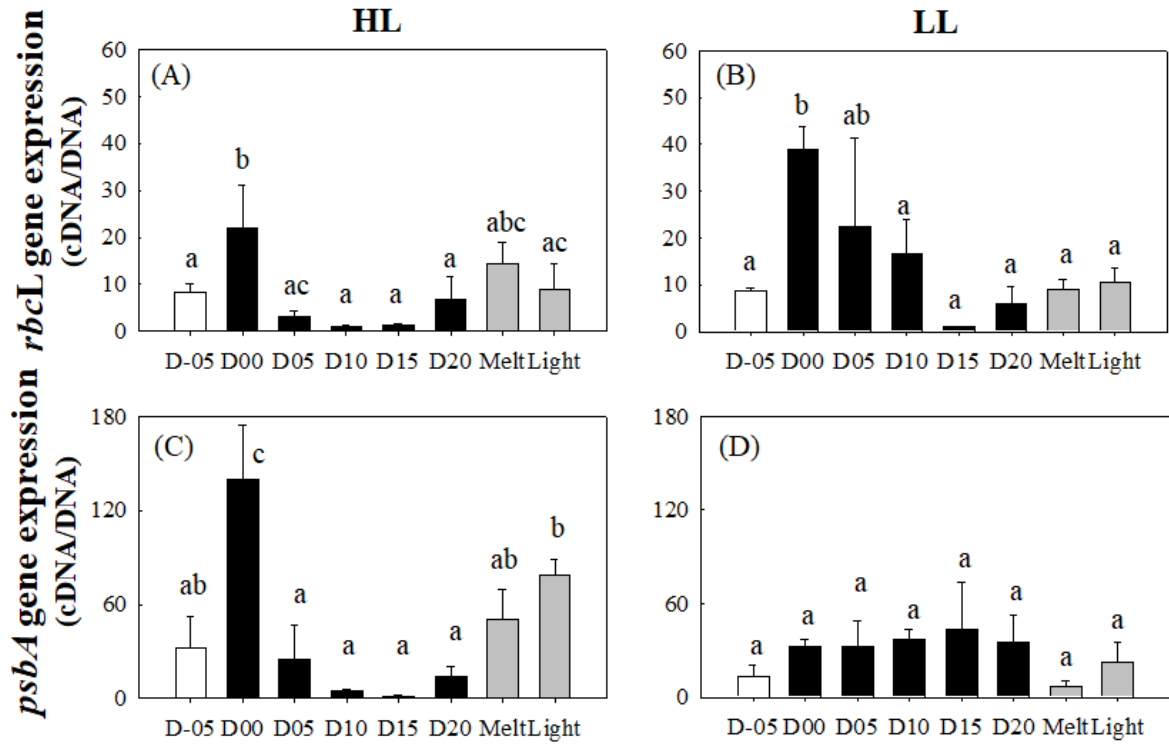
731

732 Fig. 5



733

734 Fig. 6



735

736 Fig. 7

737

738 Figure S2

739

740 **REFERENCES**

- 741 Allen, J.F. & Nilsson, A. 1997. Redox signalling and the structural basis of regulation of
742 photosynthesis by protein phosphorylation. *Physiol. Plant.* 100:863–8.
- 743 Alou-Font, E., Mundy, C.-J., Roy, S., Gosselin, M. & Agustí, S. 2013. Snow cover affects ice
744 algal pigment composition in the coastal Arctic Ocean during spring. *Mar. Ecol. Prog.*
745 *Ser.* 474: 89–104.
- 746 Arrigo, K.R. 2014. Sea ice ecosystems. *Ann. Rev. Mar. Sci.* 6:439–67.
- 747 Arrigo, K.R. 2017. Sea ice as a habitat for primary producers. In Thomas, D.N. [Ed.] *Sea Ice*.
748 3rd ed. Wiley Blackwell, pp. 352–369.
- 749 Arrigo, K.R., Mock, T. & Lizotte, M.P. 2010. Primary producers and sea ice. In Thomas,
750 D.N. & Dieckmann, G.S. [Eds.] *Sea ice*. 2nd ed. Wiley Blackwell, pp. 283–326.
- 751 Arrigo, K.R. & van Dijken, G.L. 2003. Phytoplankton dynamics within 37 Antarctic coastal
752 polynya systems. *J. Geophys. Res.* 108:3271.
- 753 Assmy, P., Ehn, J.K., Fernández-Méndez, M., Hop, H., Katlein, C., Sundfjord, A., Bluhm,
754 K., Daase, M., Engel, A., Frasson, A., Granskog, M. A., Hudson, S, R., Kristiansen, S.,
755 Nicolaus, M., Peeken, I., Renner, A. H. H., Spreen, G., Tatarek, A. & Wiktor, J. 2013.
756 Floating ice-algal aggregates below melting arctic sea ice. *PLoS One.* 8:e76599.
- 757 Bailleul, B., Rogato, A., de Martino, A., Coesel, S., Cardol, P., Bowler, C., Falciatore, A. &
758 Finazzi, G. 2010. An atypical member of the light-harvesting complex stress-related
759 protein family modulates diatom responses to light. *Proc. Natl. Acad. Sci.* 107:18214–9.
- 760 Bernard, K., Gunther, L., Mahaffey, S., Qualls, K., Sugla, M., Saenz, B., Cossio, A., Walsh,
761 J. & Reiss, C. 2018. The contribution of ice algae to the winter energy budget of juvenile
762 Antarctic krill in years with contrasting sea ice conditions. *ICES J. Mar. Sci.* 1–11.
- 763 Boetius, A., Albrecht, S., Bakker, K., Bienhold, C., Felden, J., Fernandez-Mendez, M.,
764 Hendricks, S., Katlein, C., Lalande, C., Krumpen, T., Nicolaus, M., Peeken, I., Rabe, B.,

765 Rogacheva, A., Rybakova, E., Somavilla, R., Wenzhöfer, F. & RV Polarstern ARK27-3-
766 Shipboard Science Party 2013. Export of algal biomass from the melting Arctic sea ice.
767 *Science*. 339:1430–2.

768 Boetius, A., Anesio, A.M., Deming, J.W., Mikucki, J. & Rapp, J.Z. 2015. Microbial ecology
769 of the cryosphere: sea ice and glacial habitats. *Nat. Rev. Microbiol.* 13:1–14.

770 Campbell, K., Mundy, C.J., Juhl, A.R., Dalman, L.A., Michel, C., Galley, R.J., Else, B.E.,
771 Geilfus, N. X. & Rysgaard, S. 2019. Melt procedure affects the photosynthetic response
772 of sea ice algae. *Front. Earth Sci.* 7:1–14.

773 Caron, L., Berkaloff, C., Duval, J.-C. & Jupin, H. 1987. Chlorophyll fluorescence transients
774 from the diatom *Phaeodactylum tricornutum*: relative rates of cyclic phosphorylation
775 and chlororespiration. *Photosynth. Res.* 11:131–9.

776 Cox, G.F.N. & Weeks, W.F. 1983. Equations for determining the gas and brine volumes in
777 sea-ice samples. *J. Glaciol.* 29:306–16.

778 Devos, N., Ingouff, M., Loppes, R. & Matagne, R.F. 1998. Rubisco adaptation to low
779 temperatures: a comparative study in psychrophilic and mesophilic unicellular algae. *J.*
780 *Phycol.* 34:655–60.

781 D'Haene, S.E., Sobotka, R., Bučinská, L., Dekker, J.P. & Komenda, J. 2015. Interaction of
782 the PsbH subunit with a chlorophyll bound histidine 114 of CP47 is responsible for the
783 red 77 K fluorescence of Photosystem II. *Biochim. Biophys. Acta* 1847: 1327–34.

784 Domingues, N., Matos, A.R., da Silva, J.M. & Cartaxana, P. 2012. Response of the diatom
785 *Phaeodactylum tricornutum* to photooxidative stress resulting from high light exposure.
786 *PLoS One.* 7:1–6.

787 Danon, A. & Mayfield, S.P.Y. 1991. Light regulated translational activators: identification of
788 chloroplast gene specific mRNA binding proteins. *EMBO J.* 10: 3993–4001.

789 Eiken, H. 2009. Ice sampling and basic ice core analysis. *In* Eiken, H., Gradinger, R.,

- 790 Salganek, M., Shirasawa, K., Perovich, D. & Leppäranta, M. [Eds.] *Field Techniques for*
791 *Sea Ice Research*. University of Alaska Press, pp. 117–140.
- 792 Endo, H., Sugie, K., Yoshimura, T. & Suzuki, K. 2015. Effects of CO₂ and iron availability
793 on *rbcL* gene expression in Bering Sea diatoms. *Biogeosciences*. 12:2247–59.
- 794 Endo, H., Yoshimura, T., Kataoka, T. & Suzuki, K. 2013. Effects of CO₂ and iron
795 availability on phytoplankton and eubacterial community compositions in the northwest
796 subarctic Pacific. *J. Exp. Mar. Bio. Ecol.* 439:160–75.
- 797 Ensminger, I., Busch, F. & Huner, N.P.A. 2006. Photostasis and cold acclimation: Sensing
798 low temperature through photosynthesis. *Physiol. Plant.* 126:28–44.
- 799 Falkowski, P.G. & Owens, T.G. 1980. Light-shade adaptation: Two Strategies in marine
800 phytoplankton. *Plant Physiol.* 66:592–5.
- 801 Falkowski, P.G. & Raven, J.A. 2013. *Aquatic Photosynthesis*. 2nd ed. Princeton University
802 Press, 484 pp.
- 803 Fernández-Méndez, M., Katlein, C., Rabe, B., Nicolaus, M., Peeken, I., Bakker, K., Flores,
804 H. & Boetius, A. 2015. Photosynthetic production in the central Arctic Ocean during the
805 record sea-ice minimum in 2012. *Biogeosciences*. 12:3525–49.
- 806 Fernández-Méndez, M., Wenzhöfer, F., Peeken, I., Sørensen, H.L., Glud, R.N. & Boetius, A.
807 2014. Composition, buoyancy regulation and fate of ice algal aggregates in the Central
808 Arctic Ocean. *PLoS One*. 9:e107452.
- 809 Fiedor, L., Stašiek, M., Myśliwa-Kurdziel, B. & Strzałka, K. 2003. Phytol as one of the
810 determinants of chlorophyll interactions in solution. *Photosynth. Res.* 78: 47–57.
- 811 Galindo, V., Gosselin, M., Lavaud, J., Mundy, C.J., Else, B., Ehn, J., Babin, M. & Rysgaard,
812 S. 2017. Pigment composition and photoprotection of Arctic sea ice algae during spring.
813 *Mar. Ecol. Prog. Ser.* 585:49–69.
- 814 Garrison, D.L. & Buck, K.R. 1986. Organism losses during ice melting: a serious bias in sea

815 ice community studies. *Polar Biol.* 6:237–9.

816 Goss, R. & Jakob, T. 2010. Regulation and function of xanthophyll cycle-dependent
817 photoprotection in algae. *Photosynth. Res.* 106:103–22.

818 Goss, R. & Lepetit, B. 2015. Biodiversity of NPQ. *J. Plant Physiol.* 172:13–32.

819 Horner, R.A. 1985. *Sea Ice Biota*. CRC PRESS, 215 pp.

820 Huner, N.P.A., Öquist, G. & Sarhan, F. 1998. Energy balance and acclimation to light and
821 cold. *Trends Plant Sci.* 3:224–30.

822 Jeffrey, S.W. & Hallegraeff, G.M. 1987. Chlorophyllase distribution in ten classes of
823 phytoplankton: a problem for chlorophyll analysis. *Mar. Ecol. Prog. Ser.* 35:293–304.

824 John, D.E., Patterson, S.S. & Paul, J.H. 2007. Phytoplankton-group specific quantitative
825 polymerase chain reaction assays for RuBisCO mRNA transcripts in seawater. *Mar.*
826 *Biotechnol.* 9:747–59.

827 Katayama, T. & Taguchi, S. 2013. Photoprotective responses of ice algal community in
828 Saroma-Ko Lagoon, Hokkaido, Japan. *Polar Biol.* 36:1431–9.

829 Katlein, C., Fernández-Méndez, M., Wenzhöfer, F. & Nicolaus, M. 2015. Distribution of
830 algal aggregates under summer sea ice in the Central Arctic. *Polar Biol.* 38:719–31.

831 Kennedy, F., Martin, A., Bowman, J.P., Wilson, R. & McMinn, A. 2019. Dark metabolism: a
832 molecular insight into how the Antarctic sea-ice diatom *Fragilariopsis cylindrus*
833 survives long-term darkness. *New Phytologist* 223: 675–91.

834 Kennedy, F., McMinn A. & Martin A. 2012. Effect of temperature on the photosynthetic
835 efficiency and morphotype of *Phaeocystis antarctica*. *J. Exp. Mar. Biol. Ecol.* 429:
836 7–14.

837 Kohlbach, D., Lange, B.A., Schaafsma, F.L., David, C., Vortkamp, M., Graeve, M., van
838 Franeker, J.A., Krumpfen, T. & Flores, H. 2017. Ice algae-produced carbon is critical for

839 overwintering of Antarctic krill *Euphausia superba*. *Front. Mar. Sci.* 4:1–16.

840 Kolber, Z.S., Prášil, O. & Falkowski, P.G. 1998. Measurements of variable chlorophyll
841 fluorescence using fast repetition rate techniques: Defining methodology and
842 experimental protocols. *Biochim. Biophys. Acta.* 1367:88–106.

843 Krell, A., Funck, D., Plettner, I., John, U. & Dieckmann, G. 2007. Regulation of proline
844 metabolism under salt stress in the psychrophilic diatom *Fragilariopsis cylindrus*
845 (Bacillariophyceae). *J. Phycol.* 43:753–62.

846 Kropuenske, L.R., Mills, M.M., van Dijken, G.L., Alderkamp, A., Mine Berg, G., Robinson,
847 D.H., Welschmeyer, N.A. & Arrigo, K. R. 2010. Strategy and rates of photoacclimation
848 in two major phytoplankton taxa: *Phaeocystis antarctica* (haptophyta) and *Fragilariopsis*
849 *cylindrus* (Bacillariophyceae). *J. Phycol.* 46:1138–51.

850 Kropuenske, L.R., Mills, M.M., van Dijken, G.L., Bailey, S., Robinson, D.H., Welschmeyer,
851 N.A. & Arrigo, K.R. 2009. Photophysiology in two major southern ocean phytoplankton
852 taxa: Photoprotection in *Phaeocystis antarctica* and *Fragilariopsis cylindrus*. *Limnol.*
853 *Ocean.* 54:1176–96.

854 Kuczynska, P., Jemiola-Rzeminska, M. & Strzalka, K. 2015. Photosynthetic pigments in
855 diatoms. *Mar. Drugs.* 13:5847–81.

856 Lacour, T., Larivière, J., Ferland, J., Bruyant, F., Lavaud, J. & Babin, M. 2018. The role of
857 sustained photoprotective non-photochemical quenching in low temperature and high
858 light acclimation in the bloom-forming Arctic diatom *Thalassiosira gravida*. *Front.*
859 *Mar. Sci.* 5:1–16.

860 Lavaud, J., Rousseau, B. & Etienne, A.-L. 2002. In diatoms, a transthylakoid proton gradient
861 alone is not sufficient to induce a non-photochemical fluorescence quenching. *FEBS*
862 *Lett.* 523:163–6.

863 Lazár, D., Ilík, P., Kruk, J., Strzalka, K. & Nauš, J. 2005. A theoretical study on effect of the

864 initial redox state of cytochrome *b*₅₅₉ on maximal chlorophyll fluorescence level (F_M):
865 Implications for photoinhibition of photosystem II. *J. Theor. Biol.* 233:287–300.

866 Legendre, L., Ackley, S. F., Dieckmann, G. S., Gulliksen, B., Horner, R., Hoshiai, T.,
867 Melnikov, I. A., Reeburgh, W. S., Spindler, M. & Sullivan, C. W. 1992. Ecology of sea
868 ice biota. *Polar Biol.* 12:429–44.

869 LeGresley, M. & McDermott, G. 2010. Counting chamber methods for quantitative
870 phytoplankton analysis—Haemocytometer, Palmer-Maloney cell and Sedwick-rafter cell.
871 In Karlson, B., Cusack, C. & Bresnan, E. [Eds.] *Microscopic and Molecular Methods*
872 *for Quantitative Phytoplankton Analysis*. UNESCO, pp. 25–30.

873 Lepetit, B., Volke, D., Gilbert, M., Wilhelm, C. & Goss, R. 2010. Evidence for the existence
874 of one antennae-associated. lipid-dissolved and two protein-bound pools of
875 diadinoxanthin cycle pigments in diatoms. *Plant Physiol.* 154: 1905–1920.

876 Lepetit, B., Strum, S., Rogato, A., Gruber, A., Sachse, M., Falciatore, A., Kroth, P.G. &
877 Lavaud, J. 2013. High light acclimation in the secondary plastids containing diatom
878 *Phaeodactylum tricorutum* is triggered by the redox state of the plastoquinone pool.
879 *Plant Physiol.* 161: 853–865.

880 Lizotte, M.P. 2001. The contributions of sea ice algae to Antarctic marine primary
881 production. *Am. Zool.* 41:57–73.

882 Loose, B., Miller, L.A., Elliott, S. & Papakyriakou, T. 2011. Sea ice biogeochemistry and
883 material transport across the frozen interface. *Oceanography.* 24:202–18.

884 Lyon, B. & Mock, T. 2014. Polar microalgae: New approaches towards understanding
885 adaptations to an extreme and changing environment. *Biology.* 3:56–80.

886 Maccario, L., Sanguino, L., Vogel, T.M. & Larose, C. 2015. Snow and ice ecosystems: Not
887 so extreme. *Res. Microbiol.* 166:782–95.

888 MacIntyre, H.L., Kana, T.M., Anning, T. & Geider, R.J. 2002. Photoacclimation of

889 photosynthesis irradiance response curves and photosynthetic pigments in microalgae
890 and cyanobacteria. *J. Phycol.* 38: 17–38.

891 Malnoë, P., Mayfield, S.P. & Rochaix, J.-D. 1988. Comparative analysis of the biogenesis of
892 photosystem II in the wild-type and Y-1 mutant of *Chlamydomonas reinhardtii*. *J. Cell*
893 *Biol.* 106: 609–616.

894 Martin, A., Anderson, M.J., Thorn, C., Davy, S.K. & Ryan, K.G. 2011. Response of sea-ice
895 microbial communities to environmental disturbance: An *in situ* transplant experiment in
896 the Antarctic. *Mar. Ecol. Prog. Ser.* 424:25–37.

897 Maxwell, D.P., Laudenbach, D.E. & Huner, N. 1995. Redox regulation of light-harvesting
898 complex II and *cab* mRNA abundance in *Dunaliella salina*. *Plant Physiol.* 109:787–95.

899 McKew, B.A., Davey, P., Finch, S.J., Hopkins, J., Lefebvre, S.C., Metodiev, M. V.,
900 Oxborough, K., Raines, C. A., Lawson, T. & Geider, R. J. 2013. The trade-off between
901 the light-harvesting and photoprotective functions of fucoxanthin-chlorophyll proteins
902 dominates light acclimation in *Emiliania huxleyi* (clone CCMP 1516). *New Phytol.*
903 200:74–85.

904 McMinn, A. 2017. Ice Acidification: A review of the effects of ocean acidification on sea ice
905 microbial communities. *Biogeosciences.* 14:3927–35.

906 McMinn, A., Hattori, H., Hirawake, T. & Iwamoto, A. 2008. Preliminary investigation of
907 Okhotsk Sea ice algae; taxonomic composition and photosynthetic activity. *Polar Biol.*
908 31:1011–5.

909 McMinn, A. & Hegseth, E.N. 2004. Quantum yield and photosynthetic parameters of marine
910 microalgae from the southern Arctic Ocean, Svalbard. *J. Mar. Biol. Assoc. United*
911 *Kingdom.* 84:865–71.

912 McMinn, A., Muller, M.N., Martin, A. & Ryan, K.G. 2014. The response of Antarctic sea ice
913 algae to changes in pH and CO₂. *PLoS One.* 9:e86984.

- 914 McMinn, A., Pankowski, A., Ashworth, C., Bhagooli, R., Ralph, P. & Ryan, K. 2010. In situ
915 net primary productivity and photosynthesis of Antarctic sea ice algal, phytoplankton
916 and benthic algal communities. *Mar. Biol.* 157:1345–56.
- 917 Melnikov, I.A. & Bondarchuk, L.L. 1987. Ecology of mass accumulations of colonial diatom
918 algae under drifting Arctic ice. *Oceanology.* 27:233–6.
- 919 Michel, C., Ingram, R.G. & Harris, L.R. 2006. Variability in oceanographic and ecological
920 processes in the Canadian Arctic Archipelago. *Prog. Oceanogr.* 71:379–401.
- 921 Mikkelsen, D.M. & Witkowski, A. 2010. Melting sea ice for taxonomic analysis: A
922 comparison of four melting procedures. *Polar Res.* 29:451–4.
- 923 Miller, L.A., Fripiat, F., Else, B.G.T., Bowman, J.S., Brown, K.A., Collins, R.E., Ewert, M.,
924 Frasson, A., Gosselin, M., Lannuzel, D., Meiners, K. M., Michel, C., Nishioka, J.,
925 Nomura, D., Papadimitrou, S., Russell, L. M., Sørensen, L. L., Thomas, D. N., Tison, J.-
926 L., van Leeuwe, M., Vancoppenolle, M., Wolff, E. & Zhou, J. 2015. Methods for
927 biogeochemical studies of sea ice: The state of the art, caveats, and recommendations.
928 *Elem. Sci. Anthr.* 3:000038.
- 929 Mock, T. & Hoch, N. 2005. Long-term temperature acclimation of photosynthesis in steady-
930 state cultures of the polar diatom *Fragilariopsis cylindrus*. *Photosynth. Res.* 85:307–17.
- 931 Morgan-Kiss, R.M., Priscu, J.C., Pockock, T., Gudynaite-Savitch, L. & Huner, N.P.A. 2006.
932 Adaptation and acclimation of photosynthetic microorganisms to permanently cold
933 environments. *Microbiol. Mol. Biol. Rev.* 70:222–52.
- 934 Moteki, M., Odate, T., Hosie, G.W., Takahashi, K.T., Swadling, K.M. & Tanimura, A. 2017.
935 Ecosystem studies in the Indian Ocean sector of the Southern Ocean undertaken by the
936 training vessel *Umitaka-maru*. *Polar Sci.* 12:1–4.
- 937 Mulo, P., Sakurai, I & Aro, E.-M. 2012. Strategies for *psbA* gene expression in
938 cyanobacteria, green algae and higher plants: From transcription to PSII repair. *Biochim.*

939 *Biophys. Acta* 187: 247–257.

940 Nymark, M., Valle, K.C., Hancke, K., Winge, P., Andresen, K., Johnsen, G., Bones, A.M. &
941 Brembu, T. 2013. Molecular and photosynthetic responses to prolonged darkness and
942 subsequent acclimation to re-illumination in the diatom *Phaeodactylum tricorutum*.
943 *PLoS One*. 8:e58722.

944 Öquist, G. & Huner, N.P.A. 2003. Photosynthesis of overwintering evergreen plants. *Annu.*
945 *Rev. Plant Biol.* 54:329–55.

946 Oxborough, K. & Baker, N.R. 1997. Resolving chlorophyll *a* fluorescence images of
947 photosynthetic efficiency into photochemical and non-photochemical components -
948 Calculation of *qP* and *Fv'/Fm'* without measuring *Fo'*. *Photosynth. Res.* 54:135–42.

949 Petrich, C. & Eicken, H. 2017. Overview of sea ice growth and properties. In Thomas, D.N.
950 [Ed.] *Sea Ice*. 3rd ed. Wiley Blackwell, pp. 1–41.

951 Petrou, K., Hill, R., Brown, C.M., Campbell, D.A., Doblin, M.A. & Ralph, P.J. 2010. Rapid
952 photoprotection in sea-ice diatoms from the East Antarctic pack ice. *Limnol. Oceanogr.*
953 55:1400–7.

954 Pfannschmidt, T. 2003. Chloroplast redox signals: How photosynthesis controls its own
955 genes. *Trends Plant Sci.* 8:33–41.

956 Platt, T., Gallegos, C.L. & Harrison, W.G. 1980. Photoinhibition of photosynthesis in natural
957 assemblages of marine phytoplankton. *J. Mar. Res.* 38:687–701.

958 Price, N.M., Harrison, G.I., Hering, J.G., Hudson, R.J., Nirel, P.M. V., Palenik, B. & Morel,
959 F.M.M. 1989. Preparation and chemistry of the artificial algal culture medium Aquil.
960 *Biol. Oceanogr.* 6:443–61.

961 Ralph, P.J. & Gademann, R. 2005. Rapid light curves: A powerful tool to assess
962 photosynthetic activity. *Aquat. Bot.* 82:222–37.

963 Ralph, P.J., McMinn, A., Ryan, K.G. & Ashworth, C. 2005. Short-term effect of temperature

964 on the photokinetics of microalgae from the surface layers of Antarctic pack ice. *J.*
965 *Phycol.* 41:763–9.

966 Ralph, P.J., Ryan, K.G., McMinn, A. & Fenton, G. 2007. Melting out of sea ice causes
967 greater photosynthetic stress in algae than freezing in. *J. Phycol.* 43: 948–56.

968 Riebesell, U., Schloss, I. & Smetacek, V. 1991. Aggregation of algae released from melting
969 sea ice: implications for seeding and sedimentation. *Polar Biol.* 11:239–48.

970 Rintala, J.M., Piiparinen, J., Blomster, J., Majaneva, M., Müller, S., Uusikivi, J. & Autio, R.
971 2014. Fast direct melting of brackish sea-ice samples results in biologically more
972 accurate results than slow buffered melting. *Polar Biol.* 37:1811–22.

973 Rosenbach-Belkin, V., Fisher, J.R.E. & Scherz, A. 1991. Effects of nonexitonic interaction
974 among the paired molecules on the Q_y transition of bacteriochlorophyll dimers.
975 Applications to the primary electron donors P-860 and P-960 in bacterial reaction
976 centers. *J. Am. Chem. Soc.* 113: 676–678.

977 Ryan, K.G., Tay, M.L., Martin, A., McMinn, A. & Davy, S.K. 2011. Chlorophyll
978 fluorescence imaging analysis of the responses of Antarctic bottom-ice algae to light and
979 salinity during melting. *J. Exp. Mar. Bio. Ecol.* 399:156–61.

980 Sakshaug, E. & Slagstad, D. 1991. Light and productivity of phytoplankton in polar marine
981 ecosystems: a physiological view. *Polar Res.* 10:69–86.

982 Satoh, H., Yamaguchi, Y., Watanabe, K., Tanimura, A., Fukuchi, M. & Aruga, Y. 1989.
983 Photosynthetic nature of ice algae and their contribution to the primary production in
984 Lagoon Saroma Ko, Hokkaido, Japan. *Proc. NIPR Symp. Polar Biol.* 2:1–8.

985 Schuback, N., Flecken, M., Maldonado, M.T. & Tortell, P.D. 2016. Diurnal variation in the
986 coupling of photosynthetic electron transport and carbon fixation in iron-limited
987 phytoplankton in the NE subarctic Pacific. *Biogeosciences.* 13:1019–35.

988 Schwarz, V., Andosch, A., Geretschläger, A., Affenzeller, M. & Lütz-Meindl, U. 2017.

- 989 Carbon starvation induces lipid degradation via autophagy in the model alga
990 *Micrasterias*. *J. Plant Physiol.* 208:115–27.
- 991 Smith, W.O. & Nelson, D.M. 1986. Importance of ice edge phytoplankton production in the
992 Southern Ocean. *Bioscience.* 36:251–7.
- 993 Suggett, D.J., Moore, C.M., Hickman, A.E. & Geider, R.J. 2009. Interpretation of fast
994 repetition rate (FRR) fluorescence: Signatures of phytoplankton community structure
995 versus physiological state. *Mar. Ecol. Prog. Ser.* 376:1–19.
- 996 Suggett, D.J., Prášil, O. & Borowitzka, M.A. 2011. *Chlorophyll a Fluorescence in Aquatic
997 Sciences: Methods and Applications*. Springer, New York, US, 323 pp.
- 998 Suzuki, K., Kamimura, A. & Hooker, S.B. 2015. Rapid and highly sensitive analysis of
999 chlorophylls and carotenoids from marine phytoplankton using ultra-high performance
1000 liquid chromatography (UHPLC) with the first derivative spectrum chromatogram
1001 (FDSC) technique. *Mar. Chem.* 176:96–109.
- 1002 Syvertsen, E.E. 1991. Ice algae in the Barents Sea: types of assemblages, origin, fate and role
1003 in the ice-edge phytoplankton bloom. *Polar Res.* 10:277–88.
- 1004 Szechynska-Hebda, M., Kruk, J., Gorecka, M., Karpinska, B. & Karpinski, S. 2010. Evidence
1005 for light wavelength-specific photoelectrophysiological signaling and memory of excess
1006 light episodes in *Arabidopsis*. *Plant Cell Online.* 22:2201–18.
- 1007 Taguchi, S., Saito, H., Shirasawa, K. & Hattori, H. 1997. Vertical flux of ice algal cells
1008 during the ice melting and breaking periods in Saroma Ko Lagoon, Hokkaido, Japan.
1009 *Proc. NIPR Symp. Polar Biol.* 10:56–65.
- 1010 Ting, C.S. & Owens, T.G. 1993. Photochemical and nonphotochemical fluorescence
1011 quenching processes in the diatom *Phaeodactylum tricornutum*. *Plant Physiol.*
1012 101:1323–30.
- 1013 van Leeuwe, M.A., Tedesco, L., Arrigo, K.R., Assmy, P., Campbell, K., Meiners, K.M.,

- 1014 Rintala, J.-M., Selz, V., Thomas, D. N. & Stefel, J. 2018. Microalgal community
1015 structure and primary production in Arctic and Antarctic sea ice: A synthesis. *Elem Sci*
1016 *Anth.* 6: 4.
- 1017 Yamamoto, S., Michel, C., Gosselin, M., Demers, S., Fukuchi, M. & Taguchi, S. 2014.
1018 Photosynthetic characteristics of sinking microalgae under the sea ice. *Polar Sci.* 8:385–
1019 96.
- 1020 Wood, A.M., Everroad, R.C. & Wingard, L.M. 2005. Measuring growth rates in microalgal
1021 culture. In Andersen, R.A. [Ed.] *Algal Culturing Techniques*. Elsevier, Amsterdam,
1022 Netherland, 269–285.
- 1023 Yan, D., Endo, H. & Suzuki, K. 2019. Increased temperature benefits growth and
1024 photosynthetic performance of the sea ice diatom *Nitzschia cf. neglecta*
1025 (Bacillariophyceae) isolated from Saroma Lagoon, Hokkaido, Japan. *J. Phycol.* 55:
1026 700–13.
- 1027 Yoshida, K., Endo, H., Lawrenz, E., Isada, T., Hooker, S.B., Prášil, O. & Suzuki, K. 2018.
1028 Community composition and photophysiology of phytoplankton assemblages in coastal
1029 Oyashio waters of the western North Pacific during early spring. *Estuar. Coast. Shelf*
1030 *Sci.* 212: 80–94.
- 1031 Young, J.N., Goldman, J.A.L., Kranz, S.A., Tortell, P.D. & Morel, F.M.M. 2015. Slow
1032 carboxylation of Rubisco constrains the rate of carbon fixation during Antarctic
1033 phytoplankton blooms. *New Phytol.* 205:172–81.